What determines the relationship between color naming, unique hues, and sensory singularities: illuminations, surfaces, or photoreceptors?

Article

Published Version

Open Access

What determines the relationship between color naming, unique hues, and sensory singularities: Illuminations, surfaces, or photoreceptors?

Christoph Witzel Institut Paris Descartes de Neurosciences et Cognition, Paris, France

François Cinotti Institut Paris Descartes de Neurosciences et Cognition, Paris, France

J. Kevin O'Regan Institut Paris Descartes de Neurosciences et Cognition, Paris, France

The relationship between the sensory signal of the photoreceptors on one hand and color appearance and language on the other hand is completely unclear. A recent finding established a surprisingly accurate correlation between focal colors, unique hues, and so-called singularities in the laws governing how sensory signals for different surfaces change across illuminations. This article examines how this correlation with singularities depends on reflectances, illuminants, and cone sensitivities. Results show that this correlation holds for a large range of illuminants and for a large range of sensors, including sensors that are fundamentally different from human photoreceptors. In contrast, the spectral characteristics of the reflectance spectra turned out to be the key factor that determines the correlation between focal colors, unique hues, and sensory singularities. These findings suggest that the origins of color appearance and color language may be found in particular characteristics of the reflectance spectra that correspond to focal colors and unique hues.

Introduction

How is the color signal provided by retinal photoreceptors related to the subjective experience of color and the color categories used to communicate about color? Answers to this question may elucidate the understanding of color vision as well as the general relationship between perception and language and may enrich the concept of subjective experience.

Background and relevance

Color language and color appearance

Colors are communicated through color terms, such as *red, pink,* and *purple*. These color terms categorize the multitude of perceivable colors into groups—the color categories. The corresponding categories share some statistical regularities across languages (Kay & Regier, 2003; Lindsey & Brown, 2006, 2009). Since the prototypes of the categories are representative for the whole category, they are also called *focal colors*. The prototypes of red, yellow, green, and blue are particularly stable across languages (Regier, Kay, & Cook, 2005; Webster et al., 2002). It has been argued that the prototypes of the categories are *salient* because they are easier to name and memorize than other colors (R. W. Brown & Lenneberg, 1954; Regier, Kay, & Khetarpal, 2007; Rosch Heider, 1972).

The subjective experience of color is called *color appearance*. Colors of a given appearance can always be obtained through the combination of the so-called *unique hues* (Abramov & Gordon, 1994; Valberg, 2001). Apart from black and white, these unique hues correspond to pure red, yellow, green, and blue, where the word *pure* means that the hue does not contain any of the other hues. For example, unique red is neither yellowish nor bluish (nor whitish nor blackish). There are some differences between unique hues and focal red, yellow, green, and blue. Nevertheless, these focal colors and unique hues coarsely correspond to each other.

However, color categories and focal colors are not related to the sensory mechanisms of color vision

(Bachy, Dias, Alleysson, & Bonnardel, 2012; A. M. Brown, Lindsey, & Guckes, 2011; Cropper, Kvansakul, & Little, 2013; Lindsey et al., 2010; Malkoc, Kay, & Webster, 2005; Witzel & Gegenfurtner, 2011, 2013, 2014). Unique hues do not correspond to known mechanisms of color vision (Mollon, 2009; Valberg, 2001; Wuerger, Atkinson, & Cropper, 2005; for a review see Witzel, 2011). Finally, focal colors and unique hues are not salient in a strict perceptual sense because they are not more colorful than other colors (Witzel & Franklin, 2014; Witzel, Maule, & Franklin, in prep). Taken together, the origin of color categories, focal colors, and unique hues as well as their relationship to known mechanisms of color perception remain unknown.

Sensory singularities

A new approach proposed by Philipona and O'Regan (2006) established a relationship between the color signal at the level of the photoreceptors and the focal colors and unique hues. The color signal is defined by the activation of the three photoreceptors, the cones. Each cone is particularly sensitive in a specific region of the visible spectrum of light. Since one cone is maximally sensitive to comparatively short wavelengths, one to comparatively long wavelengths, and one to wavelengths in between, they are called short-, middle-, and long-wavelength cones, or S-, M-, and L-cones, respectively. The combined excitation of these three cones carries the information about wavelength differences and hence the color signal. To refer to a triad of cone excitations, the term *LMS signal* is used here.

The three cone excitations that make up the LMS signals may be represented in a three-dimensional space—the *cone-excitation space*. Figure 1 illustrates LMS signals in this space for natural outdoor lighting, for fluorescent illuminations, for a sample of randomly constructed lights, and for monochromatic lights (see the Illumination section for details).

Low-level stages of color processing beyond the level of the photoreceptors are known (e.g., Gegenfurtner, 2003; Gegenfurtner & Kiper, 2003). However, Philipona and O'Regan's (2006) approach focuses on the LMS signal itself. Unlike previous approaches, Philipona and O'Regan (2006) did not examine how a particular LMS signal is processed in the visual system. Instead, they inspected how the variation of LMS signals is constrained by particular reflectances.

The LMS signal is determined by the light that impinges on the retina, called the *impinging light*. More precisely, it depends on the wavelength composition (here referred to as the *spectrum*) of the impinging light (henceforth referred to as the *impinging spectrum*). Impinging light can come directly from a light source
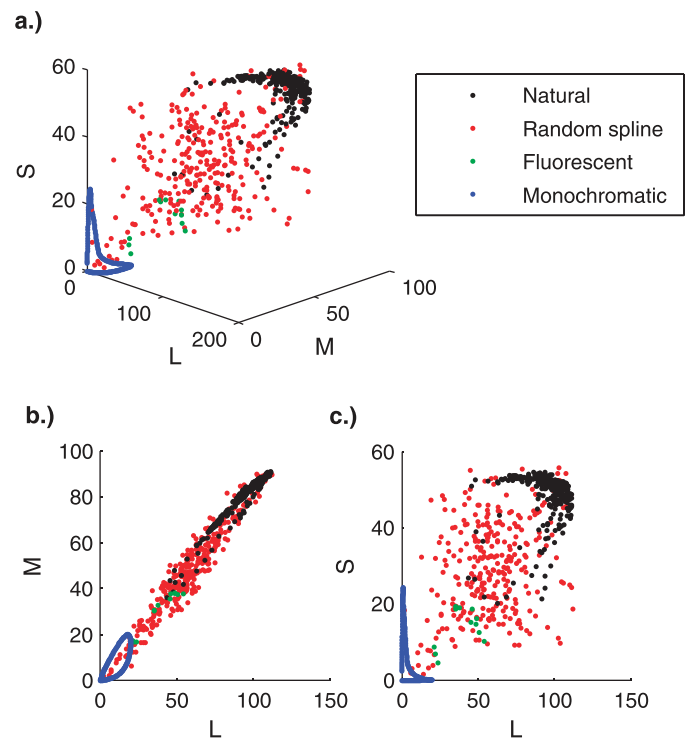

Figure 1. LMS signal for a wide range of illuminations. Axes correspond to long-, middle-, and short-wavelength cone excitations (L, M, and S, respectively). Panel a shows all three dimensions, panel b shows only L and M, and panel c shows only L and S. Natural, random-spline, fluorescent, and monochromatic lights are shown as black, red, green, and blue dots, respectively. Since the intensities of the monochromatic lights are much lower than those of the other illuminants, their LMS values are multiplied by 20 to illustrate their distribution in this plot. Note that L- and M-excitations (panel b) are strongly correlated due to the overlap of cone absorption spectra and that natural illuminants (black dots) are not uniformly distributed in cone-excitation space.

(i.e., *emitted light*), or it can be reflected off a surface (i.e., *reflected light*). In the latter case, the impinging spectrum is the product of the spectrum of the illumination (i.e., the *illuminant*) and the spectral reflectance properties of the surface (i.e., the *reflectance spectrum*). The LMS signal can be computed as the dot product between the impinging spectrum and the sensitivities of the human photoreceptors (i.e., *cone fundamentals*).

When the illumination changes, the reflected spectrum changes. The change of the reflected spectrum implies a change of the reflected LMS signal. The new approach of Philipona and O'Regan (2006) discovered that the way in which the LMS signal changes across a wide range of illuminations is particular for focal colors and unique hues.

Let us call the LMS signal that would result if the light of the illumination fell directly into the eye—that
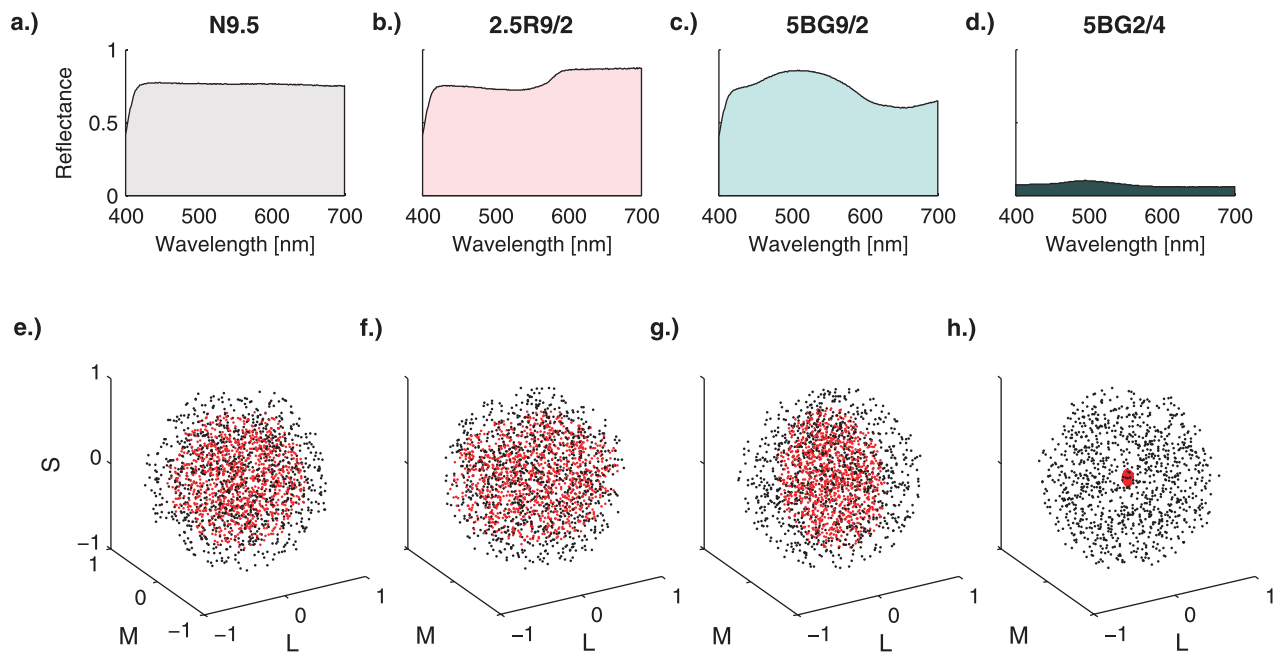
Figure 2. Reflected signal under illumination change for nonsingular surfaces. Each column corresponds to a Munsell chip with a nonsingular reflectance. The titles refer to the Munsell labels of the chips. The first row (panels a through d) shows the reflectance spectra of the respective surfaces. The *x*-axis represents wavelength (in nm), and the *y*-axis represents reflectance. The second row (panels e through h) shows LMS signals in cone-excitation space (axes as in Figure 1). Black dots correspond to uniformly distributed illuminant signals, and red dots correspond to the corresponding reflected signals of the respective Munsell chips. The uniform distribution of the illuminant signals in this graphic is used for illustration only; real LMS signals are not uniformly distributed (cf. Figure 1). Note that the reflected signal of all the chips in this graphic varies along three dimensions.

is, without being reflected by a surface—the *illuminant signal*. The light reflected off a white surface that perfectly reflects the light of the illumination would also produce the illuminant signal when falling into the eye. Let us call the LMS signal produced by the light reflected from a surface the *reflected signal*. The illuminant signal is mapped to the reflected signal in a way that is particular to the reflectance of a surface. The color of a surface may be thus seen as a map that transforms an incoming illuminant LMS signal into an outgoing reflected LMS signal. We now discuss the dimensionality of this mapping as determined by the *singularity* of the surfaces.

To illustrate the idea of singularity, let us temporarily assume that the illuminant signal could be spherically distributed as the black dots in the graphs in the lower rows of Figures 2 and 3. (In fact, as seen in Figure 1, real illuminant signals are not spherically distributed; we come back to this issue later.) The red dots in Figures 2 and 3 illustrate the reflected signals that correspond to the illuminant signals when reflected by a particular surface. The corresponding reflectance spectra of the surfaces are shown in the small graphics in the top row of Figures 2 and 3.

Figure 2 illustrates the distribution of the reflected signals for examples of surfaces that are not singular. The columns of Figure 2 (from left to right) correspond

to a white (Munsell chip N9.5), a slightly pinkish (Munsell chip 2.5R9/2), a light turquoise (Munsell chip 5BG9/2), and a dark turquoise (Munsell chip 5BG2/4) surface. For all these surfaces, the distribution of the reflected signal (red dots in panels e through h) covers all three dimensions of cone-excitation space. This is also true for the distribution of red dots in panel h. The variability of the red dots in panel h is strongly reduced because much less light is reflected by the dark surface in panel d than by the light surfaces in panels a through c. Despite the smaller variability, the distribution in panel h is three-dimensional.

In contrast, Figure 3 illustrates the distribution of the reflected signals for examples of surfaces that are singular. Singular surfaces produce distributions of reflected signals that are restricted to a subspace of the LMS space with a lower dimensionality than the illuminant signal. For the surfaces in Figure 3, one or even two dimensions of the distributions of the reflected signal are negligible. The columns of Figure 3 correspond to a red (Munsell chip 5R4/14), a yellow (Munsell chip 2.5Y8/16), a green (Munsell chip 10GY5/12), and a blue (Munsell chip 7.5PB3/12) surface. The reflected signal (red dots) of the focal red (panel a), green (panel c), and blue (panel d) surfaces vary quasi one-dimensionally—that is, along a line in three-dimensional cone-excitation space. The reflected signal
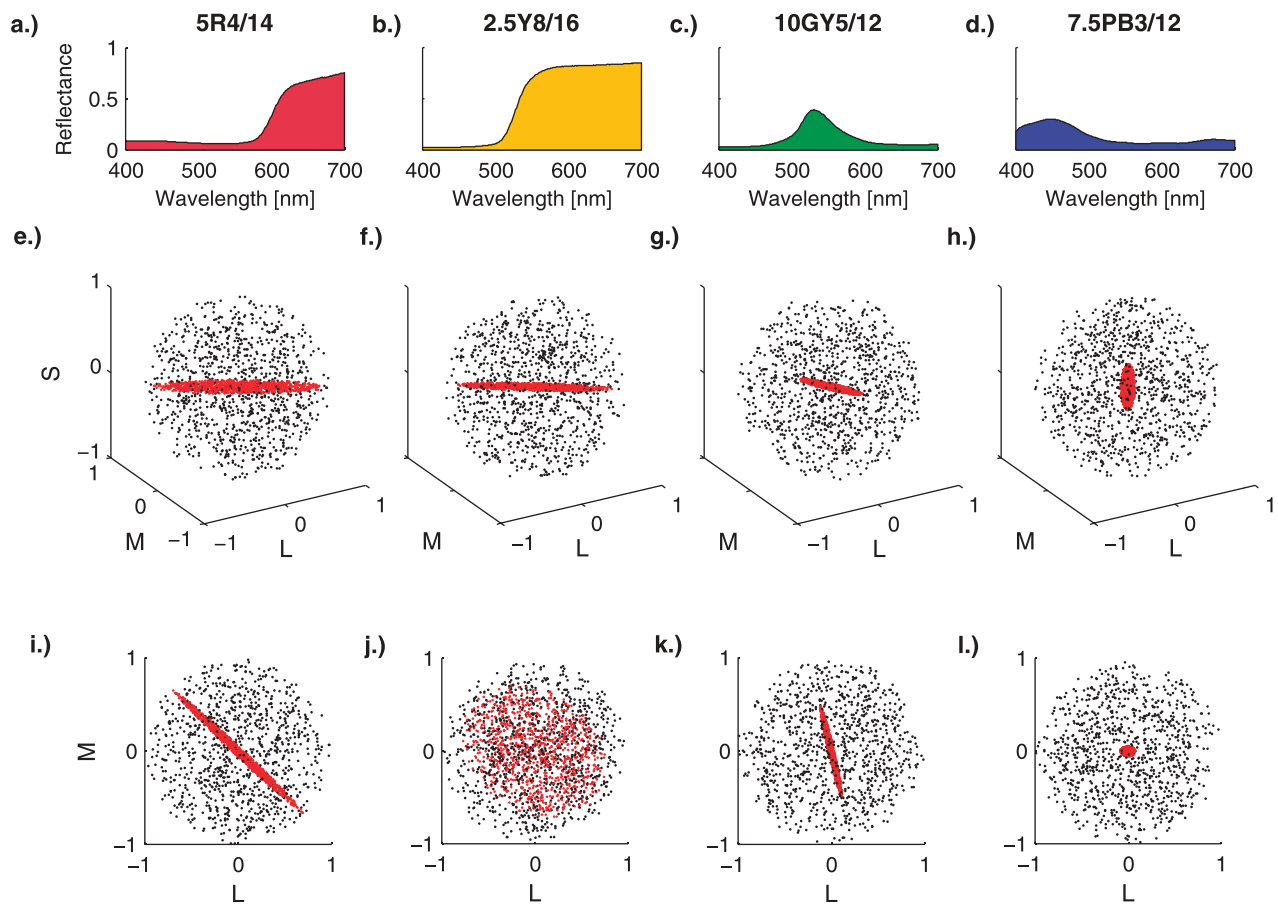
Figure 3. Reflected signal under illumination change for singular surfaces. The variation of the reflected signal (red dots) of surfaces with the highest singularity indices is illustrated. The format of the first (panels a through d) and second (panels e through h) rows is as in Figure 2; the third row (panels i through l) shows the variation in the LM plane to highlight differences in dimensionality across the surfaces. In contrast to the nonsingular surfaces in Figure 2, the variation of these singular surfaces is almost one-dimensional (red, green, and blue) or two-dimensional (yellow; cf. panels f and j).

of the yellow surface (panel b) varies quasi two-dimensionally—that is, across a plane in cone-excitation space. To further illustrate this observation, the second and third rows of Figure 3 show the variation of the reflected signal from two perspectives. Note in particular that the reflected signal of the yellow surface is seen from the profile and from above the plane, hence illustrating the planar distribution. The mapping of the illuminant signal onto the reflected signal by these surfaces is approximately singular in a mathematical sense.

As mentioned above, real illuminant signals and LMS signals in general are not uniformly distributed in cone-excitation space. As shown in Figure 1, L- and M-cone excitations are always correlated due to the overlap of the L- and M-cone sensitivities. As a result, the distribution of the real illuminant signals in Figure 1 is close to a plane and is not spherical like the distribution used for illustration purposes in Figures 2 and 3.

However, the fact that LMS signals are restricted in their variation does not undermine the observation that the mapping of the illuminant to the reflected signal is singular for certain surfaces. Indeed, the singularities of the surfaces would be the same if we used decorrelated, orthogonal signals, such as $L - M$, $L + M$, and S, instead of the cone excitations L, M, and S (cf. Supplementary Figures S1 through S3 and Supplementary Figure S4a in the Decorrelated signals section of the supplementary materials).

Philipona and O'Regan (2006) observed the notable fact that the most singular surfaces were almost the same as the focal colors determined in the World Color Survey (Regier et al., 2005). Philipona and O'Regan (2006) also showed that, under certain assumptions, this observation also holds for surfaces that correspond to unique hues. Hence, surfaces with focal colors and unique hues are more singular in a mathematical sense than other surfaces.

Vazquez-Corral, O'Regan, Vanrell, and Finlayson (2012) further supported this observation. In a follow-

Witzel, Cinotti, & O'Regan

up study, they showed that the variation of the reflected signal may be represented by three new sensors, which they called *spectrally sharpened sensors*. The number of spectrally sharpened sensors that respond to a light directly reflects the singularity of the surfaces. Hence, focal colors and unique hues excited fewer than three of the spectrally sharpened sensors.

Sensorimotor theory of color appearance and naming

These findings imply that focal and unique red, yellow, green, and blue have particular properties under changing illuminations that distinguish these colors from all the other colors. The sensory singularity of these surfaces suggests that the way the reflected signal from these surfaces changes across illuminations is more predictable, in the sense that it varies along fewer dimensions.

Another way of thinking about singularities is to realize that the way singular surfaces affect incoming light can be described by only one or two parameters instead of the three parameters (the three eigenvalues) that would be necessary for most surfaces. Seen from this point of view, we can then understand that achromatic surfaces should also be considered special: The way they affect incoming light can be described by a single parameter—namely, the surface lightness. The LMS value of the incoming light is multiplied by the lightness to obtain the LMS value of the light reflected off the surface.

Consequently, the LMS signal of surfaces with those colors (red, yellow, green, blue, and achromatic colors) might be more reliable across illuminations, and they may act as points of reference, or *perceptual anchors,* for the identification of colors across illumination changes. This might explain why these colors are associated with a particular subjective experience and why the color categories used in communication organize around these particular color sensations.

Due to adaptation and other functions of color constancy, changes of the LMS signal do not necessarily correspond to perceived color changes. However, singularities may play a much more important role under fast changes of illumination. In this case, the observer cannot completely adapt to the illumination. In the natural environment, illuminations change mostly slowly by themselves (e.g., daylight from dawn to dusk). Fast changes in illumination occur when the observer moves the surfaces (e.g., from shadow to sunlight or under a canopy of trees). Fast changes also happen when the observer tilts a surface under different simultaneous illuminations. Hence, the sensory singularities that relate surfaces to color categories become evident mainly when the observer interacts with objects in a way that shows their surfaces under different illuminations.

Thus, according to this approach, color appearance and color language originate through the observer's interaction with the visual environment. The particular stability of the light reflected off focal color surfaces under different illuminants, as expressed by their singularity, may explain why the focal red, yellow, green, and blue are chosen as special color prototypes across languages and why these colors act as unique hues in color appearance. In this case, color language and the subjective experience of color would be shaped by the observers' interaction with the visual environment, as suggested by the sensorimotor theory of visual experience (O'Regan, 2011; O'Regan & Noe, 2001a, 2001b; Philipona & O'Regan, 2006).

Objective

The previous studies (Philipona & O'Regan, 2006; Vazquez-Corral et al., 2012) that provided evidence for the relationship between focal colors, unique hues, and sensory singularities used particular kinds of illuminants and surfaces and the sensitivities of human photoreceptors. More precisely, they used natural illuminants and a limited set of standard color chips (Munsell chips) with particular properties (maximal saturation). As we explain in detail in the respective sections below, those illuminants, reflectance spectra, and human photoreceptors have particular properties that might be responsible for the relationship that was observed between sensory singularities, focal colors, and unique hues.

The question arises of whether this relationship exists only for this particular selection of natural illuminants, human photoreceptors, and maximally saturated Munsell chips. In particular, if this relationship exists only for human photoreceptors, this would highlight the importance of the characteristics of the human visual system for the singularities of focal colors and unique hues. In contrast, if the relationship holds only for natural illuminants or the reflectances of maximally saturated Munsell chips, this would emphasize the role of factors in the visual environment. Finally, the dependence of this relationship on a combination of these factors may indicate that the visual system is adapted to the visual environment in a way that results in the particular pattern of singularities that is related to focal colors and unique hues. In any case, results will clarify which of these three kinds of factors are worth being studied more closely in future research.

The present study investigates whether the relationship between sensory singularities, focal colors, and unique hues depends on the characteristics of the illuminants, the reflectances, or the sensors. For this purpose, we examine this relationship (a) using

different kinds of artificial illuminants, (b) using sensors with spectral sensitivities other than the human photopigments, and (c) with different sets of reflectance spectra that still result in colors similar to Munsell chips under neutral illumination. Preliminary results of these investigations were previously presented (Witzel, Cinotti, & O'Regan, 2014). In the supplementary materials, we also provide a set of MatLab functions for computing sensory singularities. These functions are slightly different from those used in previous publications in a way that allows for more robust calculations across the different conditions investigated in the present article.

General method

In our investigations, the results of Philipona and O'Regan (2006) were the reference to evaluate how LMS signal variability is related to focal colors and unique hues when using different illuminants, reflectances, and sensors. For this reason, we used largely the same calculations and data as Philipona and O'Regan (2006). As explained below, we slightly modified the algorithms and used a different data set for the human photoreceptors. These slight deviations from the original method were done to improve and generalize the method for the analyses of the present article. However, these modifications did not affect the patterns obtained with the original method of Philipona and O'Regan (2006).

Data

Illuminants, photoreceptors, and reflectances

Following Philipona and O'Regan (2006) as well as Vazquez-Corral et al. (2012), we used measured and simulated daylight illuminants. The sample of measured illuminants included 99 measurements of daylight spectra in Grenada (Romero, Garcia-Beltran, & Hernandez-Andres, 1997) and 238 daylight spectra of the forests in Maryland (Chiao, Cronin, & Osorio, 2000). The simulated daylight illuminants were based on the three basis functions specified by Judd and colleagues (Das & Sastri, 1965; Dixon, 1978; Judd et al., 1964; Romero et al., 1997; Sastri & Das, 1966, 1968; for a review see Maloney, 1999). The parameters that combine these basis functions were fixed so that the resulting spectra produced chromaticities within the area span by standard illuminants D45, D65, and D85. As in Philipona and O'Regan (2006), illuminant spectra were normalized so that their maximum corresponded to 1.

In order to represent the sensitivity of the human photoreceptors, Philipona and O'Regan (2006) applied

10° Stiles and Burch color-matching functions (Stiles & Burch, 1959), and Vazquez-Corral et al. (2012) used the cone fundamentals of Smith and Pokorny (1975). We used the 2° Stockman-Sharpe cone fundamentals of Stockman and Sharpe (2000) for the simple reason that they directly refer to the sensitivity of the human photoreceptors and are particularly precise. In any case, the results do not depend on which measurements of cone sensitivities are used (for details, see the Sensors section).

The reflectances for glossy Munsell chips were retrieved from the database of the Joensuu Color Group (Kohonen, Parkkinen, & Jaaskelainen, 2006; Parkkinen, Hallikainen, & Jaaskelainen, 1989), which is now available via the University of Eastern Finland (http://www.uef.fi/fi/spectral). The Munsell system arranges color chips by their hue (*Munsell hue*), lightness (*Munsell value*), and chroma (*Munsell chroma*; Munsell Color Services, 2007). To establish the relationship between singularities and focal colors, the reflectance spectra of a set of 320 maximally saturated Munsell chips were used. The Munsell chips varied in 40 levels of hue and eight levels of lightness (Munsell value = 2–9) and had maximal Munsell chroma. Throughout this article, the set of Munsell chips is arranged vertically by its eight lightness levels and horizontally by its 40 hue levels. Figure 4a illustrates the variation of Munsell chroma across the 8×40 chips. This choice of Munsell chips allows the comparison of the singularities of these reflectances with measurements of focal colors and unique hues.

Focal colors and unique hues

Data on focal colors were obtained from the *World Color Survey*, a cross-cultural study on color naming (Regier et al., 2005). In this study, observers from 110 nonindustrialized societies were asked to indicate the typical colors of the color categories that correspond to the basic color terms of their language. They could choose among the aforementioned set of 320 chromatic and 10 achromatic (grayscale) Munsell chips. The relative frequencies of prototype choices across all observers indicate the *focality* of the Munsell chips—that is, the extent to which their color is focal. The contours in Figure 4b illustrate the relative frequency of prototype choices across the set of 320 chromatic Munsell chips; it is plotted the same way as in figure 2 of Regier et al. (2005) and as in the corresponding graph in figure 3 of Philipona and O'Regan (2006).

The modes of these focal color choices (innermost contours) coincide with the prototypes of red, yellow, green, and blue in English (for details see figure 2 in Regier et al., 2005). They also coarsely coincide with the unique hues. According to Kuehni, Shamey, Mathews, and Keene (2010), Munsell chips 5R4/14,

5Y8/14, 2.5G5/12, and 2.5PB5/12 correspond to unique red, yellow, green, and blue, respectively (see table 1 in Kuehni et al., 2010). These Munsell chips are highlighted as black circles in Figure 4 and subsequent contour plots (Figures 6, 7, 10, and 14).

Calculation of singularity

Philipona and O'Regan's (2006) approach to determining the singularities of the reflectances consists of three steps. The MatLab functions section in the supplementary materials provides the functions we used to implement these steps in the present study.

Step 1: Reflected and illuminant signals

The first step concerns the relationship between the illuminant LMS signal and the reflected LMS signal across different illuminations. A priori, the maps that link illuminant LMS signals to reflected LMS signals could be arbitrary, taking illuminant LMS triples into arbitrary reflected LMS triples. But what Philipona and O'Regan (2006) observed was the surprising result that for most surfaces, the maps were very accurately linear. The linear transformation between the illuminant signals and reflected signals may be characterized by a 3 × 3 *transformation matrix* A that converts the illuminant signals into the reflected signals of a given surface across all illuminants. The matrix A that does this with minimum error (maximum variance explained) can be obtained by linear regression. Philipona and O'Regan (2006) showed that the residual variation that is not explained through the linear transformation is almost zero (no more than around 0.015 of the total variance) for each of the reflectances (cf. figure 1 in Philipona & O'Regan, 2006). Hence, reflected signals of a given surface across a wide range of illuminations may be approximated with almost perfect accuracy by a linear transformation of the LMS signal of those illuminations. The matrix A that accomplishes the linear transformations is specific to a given surface reflectance.

Our function "A_maker" computes the linear regression and provides the transformation matrix A. This function uses a slightly different least squares method than the original algorithm of Philipona and O'Regan (2006). For details, see the MatLab functions section in the supplementary materials.

Step 2: Sensory singularities

The second step concerns the properties of the matrix A that defines the linear transformation. The three cone excitations that make up the illuminant and reflected LMS signals may be represented in a three-dimensional space—the cone-excitation space. In general, a 3 × 3 matrix will take a point in three-dimensional space and project it into another point in three-dimensional space. For a typical matrix A, when the illuminant varies over the whole cone-excitation space, the reflected signal will also vary across the whole cone-excitation space (cf. Figure 2).

However, sometimes a matrix projects the three-dimensional illuminant signal into a two-dimensional or one-dimensional subspace of three-dimensional cone-excitation space. Such matrices are called singular matrices. With surfaces corresponding to matrices A that are singular, the reflected signal will be restricted to a plane or a line within the three-dimensional cone-excitation space (cf. Figure 3). The degree to which this happens is measured by the *eigenvalues* of the matrix A, as obtained by *eigenvalue decomposition* of the matrix A. When an eigenvalue is close to zero, there is an axis along which the variation of the reflected signal will be very small. Illuminant signals transformed by matrices with one near-zero eigenvalue are projected into reflected signals restricted to a plane in cone-excitation space. When two eigenvalues are close to zero, there are two axes along which the variation of the reflected signal is small. Illuminant signals transformed by matrices with two near-zero eigenvalues are projected into reflected signals almost restricted to a line in cone-excitation space.

Our function "ev_calculator" calculates the eigenvalues of the transformation matrix A for each reflectance (see the MatLab functions section in the supplementary materials). The algorithm of this function is equivalent to the one of Philipona and O'Regan (2006).

Step 3: Singularity index

The third step consists of the calculation of a *singularity index*. In order to compare singularities of the matrices corresponding to different surfaces, an index was needed to assess the singularity of a transformation matrix A with a single number.

When one or two eigenvalues are zero, the transformation is unambiguously two- or one-dimensional, respectively. The major challenge consists of evaluating when an eigenvalue can be judged as being close to zero.

To solve this problem, Philipona and O'Regan (2006) proposed the following method. They ordered the three eigenvalues by their size (similar to what is done in a principal component analysis), with the last eigenvalue being closest to zero. If this last eigenvalue is negligibly small compared with the other two values, the ratio between the second largest eigenvalue and this last eigenvalue will be large and the transformation through matrix A will be approximately two-dimensional. However, if two values are close to zero, then
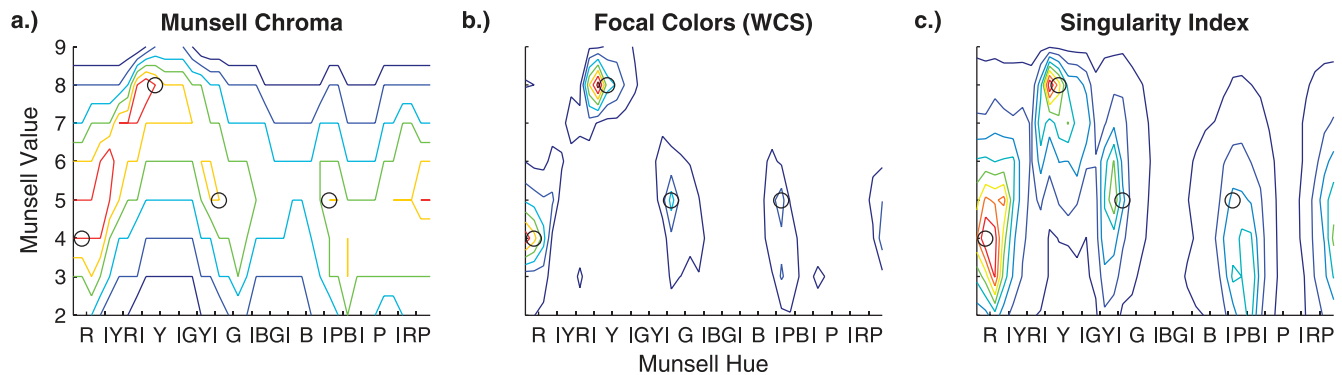
Figure 4. Munsell chips used by Philipona and O'Regan (2006). Graphics show Munsell chips arranged by their hue (*x*-axis) and lightness (*y*-axis), which are defined as Munsell hue and Munsell value, respectively, in the Munsell Color System (Munsell Color Services, 2007). Black circles highlight the Munsell chips that Kuehni et al. (2010) identified as unique red, yellow, green, and blue (from left to right). In panel a, contours refer to Munsell chroma; in panel b, they refer to the relative frequencies of prototype choices (i.e., focality) in the World Color Survey (figure 2 in Regier et al., 2005); and in panel c, they refer to the singularity indices. Red contours correspond to high values, green correspond to medium values, and blue correspond to low values. Note that the local peaks (innermost contours) are at similar locations in all three graphs and that they are close to the unique hues (black circles).

the ratio between the first and the second eigenvalue will be large and the transformation through matrix A will be approximately one-dimensional.

Philipona and O'Regan (2006) decided not to make a difference between cases when the reflected signal was restricted to a one- or two-dimensional subspace of cone-excitation space (e.g., between the first and second columns in Figure 3). Instead, they focused on whether the reflected signal could occupy a three-dimensional region. For this reason, they defined a *singularity index* as the maximum of the two eigenvalue ratios. This singularity index gives an indication of the degree to which the matrix compresses incoming illuminant signals into either a two-dimensional or a one-dimensional subspace of three-dimensional cone-excitation space. The higher this singularity index, the less three-dimensional is the space occupied by the illuminant signal in cone-excitation space.

Our function "si_calculator" determines the singularity index based on the eigenvalues of the transformation matrices (see the MatLab functions section in the supplementary materials). The algorithm of this function is equivalent to the one of Philipona and O'Regan (2006).

Analyses

The singularity index allows the comparison of singularities across the reflectances. The singularity indices for the Munsell chips as calculated with our functions are illustrated by Figure 4c. For comparison, those calculated by Philipona and O'Regan (2006) and through the approach of Vazquez-Corral et al. (2012) are provided in Supplementary Figure S4b and c.

Philipona and O'Regan (2006) found a relationship between singularity on the one hand and focal colors and unique hues on the other. Through visual inspection they observed that the pattern of singularities across Munsell chips (our Figure 4c) looked similar to the pattern of focal color choices across those Munsell chips (Figure 4b). In particular, high singularity indices coincided with Munsell chips that were chosen most often as typical colors in the World Color Survey; that corresponded to the most typical red, yellow, green, and blue in English; and that corresponded to the unique hues (black circles in Figure 4). Figure 4b also illustrates potential differences between the exact location of the peaks of focal color choices and unique hues. However, in any case, focal colors and unique hues are sufficiently similar to both be related to the peaks of the singularity index in Figure 4c.

In order to quantify the relationship between singularities and focality, we calculated the correlation between the relative frequencies of focal color choices and the singularities across the 320 Munsell chips. Figure 5a illustrates the relationship between singularities (Figure 4c) and focality (Figure 4b) for the natural illuminants, human photoreceptors, and maximally saturated Munsell chips when using our algorithms and data. (For comparison, corresponding figures for the original results of Philipona and O'Regan, 2006, and for the compact singularity index of Vazquez-Corral et al., 2012, are provided in Supplementary Figure S5.) The correlation between singularities and focal color choices explained 41% of the total variance ($r = 0.64$, $p < 0.0001$). This correlation quantifies the similarity between the patterns of focality and singularities in panels b and c of Figure 4.

Main tests

In the present study, we investigated whether the relationship between singularities, focal colors, and unique hues depends on the characteristics of the natural illuminants, the human photoreceptors, and the reflectances of the Munsell chips. For this purpose, we analyzed (a) how changes to the illumination, the sensors, and the reflectances affect the singularity pattern and (b) how the resulting singularities relate to focal color choices and unique hues.

First, to evaluate the changes in the pattern of singularities, we compared singularities for new illuminants, sensors, or reflectances with the singularities in Figure 4c that resulted from Philipona and O'Regan's (2006) illuminants, sensors, and reflectances. We calculated correlations across Munsell chips between the singularity indices in Figure 4c and the respective singularity indices obtained with other illuminants, sensors, or reflectances in order to quantify and statistically evaluate the similarity between patterns of those two sets of singularities.

Second, we tested whether the relationship between singularities and focal colors holds despite changes to the illuminants, sensors, or reflectances. For this purpose we calculated the correlations across Munsell chips between singularity indices and focality. This is the same kind of correlation as described and illustrated in Figure 5a for the results of Philipona and O'Regan (2006), but here they were calculated for singularities based on illuminants, sensors, and reflectances that differed from those of the previous studies. Finally, unique hues were compared with the peaks of singularities. They also serve as points of reference across graphics with different singularity patterns.

Criteria

The main criterion for both kinds of correlations was whether those correlations were significant. Due to the large sample size ($N = 320$ Munsell chips), the t test for the correlations had a high statistical sensitivity (or power). As a result, any correlation ≥ 0.11 (i.e., explaining $>1\%$ of the variance) became significant in these tests. Moreover, when accepting a beta (or Type II) error of 0.05 in the absence of a significant correlation in those tests, possible correlations that the tests missed may amount to only $r = 0.19$, explaining 3.4% of the variance. Hence, in the case of nonsignificant results, we consider that changing the illuminants, the sensors, or the reflectances destroyed the pattern of singularities originally observed with daylight illuminants, cone sensitivities, and maximally saturated Munsell chips.

However, in order to further qualify the impact of changing illuminants, sensors, and reflectances on the pattern of singularities, we also examined whether the variance explained by the resulting correlation coefficients differed significantly from a 50% criterion that was defined as follows. For the first kind of correlations between two sets of singularity indices, the 50% criterion simply corresponds to correlation coefficients of $r = 0.71$, which explain 50% of variance. For the second kind of correlations between singularities and focal colors, the reference for the 50% criterion was the original correlation in Figure 5a, which explained 41% of the variance. For this reason, the 50% criterion corresponds to a correlation coefficient of $r = 0.45$, which explains half of the 41%—namely, 20.4% of the variance. If a correlation explained significantly more variance than that defined by the 50% criterion, the pattern of singularities was considered to be similar to the one originally obtained and the relationship to focal colors was considered to be high. If a correlation was significantly below the 50% criterion, the respective change of illuminants, sensors, or reflectances is reported to have a strong effect on the pattern of singularities or the relationship between singularities and focal colors.

For correlations between singularities and focal colors, we also inspected whether they were significantly lower than the ones obtained with daylight illuminants, cone sensitivities, and maximally saturated Munsell chips. (This did not make sense for the correlations between singularities because almost all correlations below 1 are significantly different from 1.)

These criteria are illustrated through the red bands in Figures 8, 11, and 15. The first bar in these figures illustrates the correlation obtained with daylight illuminants, cone sensitivities, and maximally saturated Munsell chips, and the red bands show 0.95 confidence intervals around 50% and 100% of the variance. All the statistical comparisons between correlations were done through z tests using Fisher's z transformations (Fisher, 1921).

Illumination

Examples of the natural illuminants used by Philipona and O'Regan (2006) and Vazquez-Corral et al. (2011) are shown in Figure 6a. Such natural illuminant spectra can be accurately represented using three basis functions (Das & Sastri, 1965; Dixon, 1978; Judd et al., 1964; Romero et al., 1997; Sastri & Das, 1966, 1968; for a review see Maloney, 1999). For this reason, the first three principal components of the natural illuminants used here almost completely (98%) explain the variance of the spectra (Figure 6e).

Philipona and O'Regan (2006) demonstrated that it is analytically true that the transformation between illuminant and reflected signal can be modeled by a $3 \times$
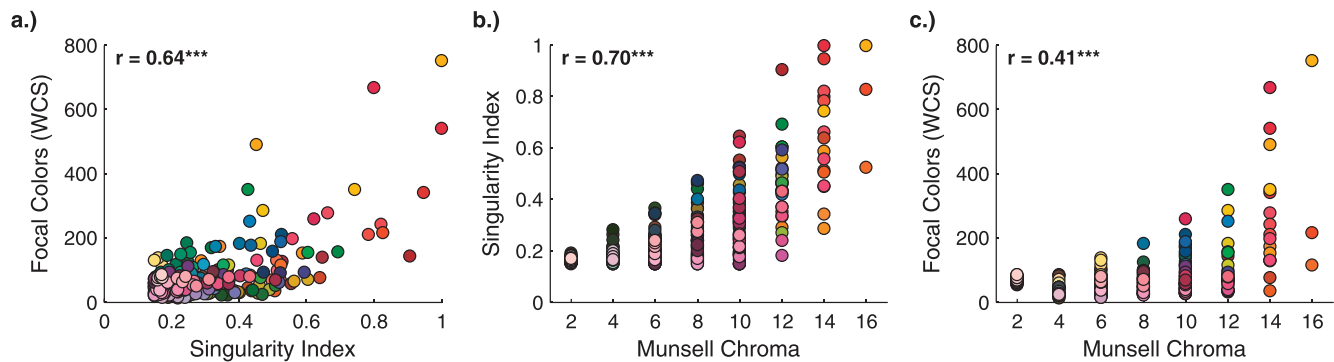
Figure 5. Correlations across Munsell chips. Each colored disk corresponds to one of the Munsell chips in the graphs of Figure 4. Axes with the label "Focal colors" refer to the number of prototype choices in the World Color Survey (Regier et al., 2005), as shown in Figure 4b. Panels a through c illustrate the correlation between singularity index and focal colors (data in Figure 4b, c), between Munsell chroma and singularity index (data in Figure 4a, c), and between Munsell chroma and focal colors (data in Figure 4a, b), respectively. Correlation coefficients are given in the upper left corner of each panel; $***p < 0.0001$. The correlation in panel a quantifies the results of Philipona and O'Regan (2006) as explained in the General method section; the correlations in panels b and c are discussed in the Surfaces section.

3 matrix when the illuminant spectra can be represented by three basis functions. We reproduce the mathematical proof in the Mathematical proof for three basis functions section of the supplementary materials. Consequently, the linear approximation of the transformation between illuminant and reflected signals is highly accurate in the case of natural illuminants. This is illustrated by Figure 6i, which shows the high similarity of the reflected LMS signal and its linear approximation when using the natural illuminants of Philipona and O'Regan (2006). Small differences between illuminant and reflected signals are due to the fact that empirical illuminants are only approximated and not completely represented by three basis function.

The first question is whether the approximation through that linear transformation is also accurate when using artificial illuminants that may not be decomposed into three basis functions. The second question is whether the distribution of singularities reproduced with the artificial illuminants is the same as that obtained with the natural illuminants. The third question is whether the singularities obtained with the artificial illuminants are related to focal colors and unique hues.

Method

As one set of artificial illuminants, we used 12 standard illuminants (F1–F12), which simulate fluorescent lights. The spectra are displayed in Figure 6b. Like the natural illuminants, these fluorescent illuminants may be represented by three principal components that explain 99% of the variance (Figure 6f). However, the spectra of the fluorescent illuminants in Figure 6b are fundamentally different from those of the

natural illuminants in Figure 6a. In particular, they have several pronounced peaks in their spectral power distributions, and they have rather narrow-band spectra compared with natural illuminants. Hence, these fluorescent spectra allowed for testing whether the pattern of singularities found with natural spectra holds for indoor illumination with spectra that strongly differ from natural ones.

As a second set of artificial illuminants, we used 300 random-spline illuminants that were produced as follows. For each random spectrum, 10 data points ($x =$ wavelength, $y =$ relative intensity) were randomly created within the visible spectrum (i.e., between 400 and 700 nm). A random value along the y-axis (intensity) was determined at the beginning and end of the spectrum. A smooth curve was interpolated through cubic splines. The values at the beginning and end of the spectrum prevented intensities from systematically increasing at the beginning and end of the spectrum because cubic functions increased to positive or negative infinity. Figure 6c shows 12 sample random spline spectra.

Figure 6g shows the first three principal components of these random-spline illuminants. They represent only 54% of the variance (of random-spline illuminants). Fifteen principal components are necessary to represent 98% of the variance of random-spline illuminants. Hence, in contrast to natural and fluorescent illuminants, random-spline illuminants may not be represented by only three linear basis functions. In this way, this set of random illuminants allowed for testing whether results depend on whether illuminants may be decomposed into three basis functions. Moreover, these random-spline illuminants include a large range of different spectra. They include both very narrow-band ("peaky") and broad-band spectra (cf. Figure 6c). In

this way, this sample of illuminants allows for testing more generally whether the pattern of singularities found with natural illuminants may be reproduced for a large range of possible illuminants.

Finally, a third set of artificial illuminants consisted of monochromatic lights (Figure 6d shows examples). Each of these illuminants consists of a Gaussian function centered at a different integer wavelength and with a standard deviation of 0.3 nm. The set consisted of illuminants for all integer wavelengths between 400 and 700 nm, resulting in overall 301 illuminants. These illuminants are extremely peaky and narrow band. Furthermore, they cannot be represented using three principal components (here such components would capture only 3% of the variance; cf. Figure 6h).

To examine the effect of sampling illuminations from only parts of the visual spectrum, we also analyzed four "sparse samples" of of monochromatic illuminants (cf. Figure 7). Sparse samples consisted of sets of only 13 monochromatic illuminants. One of the four sets consisted of Gaussians sampled evenly every 25 nm across the whole visible spectrum (Figure 7a). A second set was sampled in the short-wavelength (or "left") region of the spectrum at integer wavelengths between 420 and 432 nm (Figure 7b). The third set covered the medium-wavelength (or "center") region at integer wavelengths between 543 and 555 nm (Figure 7c), and the last set consisted of long-wavelength (or "right") samples at 668 to 680 nm (Figure 7d). For computational reasons, these Gaussians had a standard deviation of 15 nm.

The sets of monochromatic illuminations were used to test specifically whether the pattern of singularities found with natural spectra holds for narrow-band, peaky illuminant spectra and to explore under which conditions the pattern breaks down.

For the sensors and the reflectances, Stockman-Sharpe cone fundamentals and maximally saturated Munsell chips were used, as explained in the General method section.

Results

Linear approximation of reflected LMS signal

The third row of Figure 6 (panels i through l) illustrates the similarity between the actual reflected LMS signal and its linear approximation through the transformation matrix A. Note that for illustration purposes the reflected signal is shown for a sample reflectance (the red Munsell chip 5R4/14 of Figure 3a) and the sample illuminants shown in the first row of Figure 6. For all sets of illuminations considered here, the matrices A calculated for all Munsell chips extremely accurately accounted for the transformation from illuminant to reflected LMS signal (cf. Supplementary Table S1). The average variance ex-

plained by the linear approximation with transformation matrix A was $R^2 = 99.2\%$ for fluorescent, $R^2 = 98.9\%$ random-spline, and 95.7% for monochromatic illuminants. This was almost as high as for natural illuminants ($R^2 = 99.9\%$). For sparse sets, the variance explained by the linear approximation was 100%. These results indicate that the reflected signal can be approximated with high accuracy for fluorescent, random-spline, and monochromatic illuminants.

For fluorescent illuminants, this result may be explained by the fact that they can be represented through three linear basis functions (cf. Figure 6f), as was the case for the natural illuminants (Figure 6e). However, random-spline and monochromatic illuminants cannot be represented by three linear basis functions (Figure 6g, h). Hence, the fact that we can find an adequate linear approximation defined by the transformation matrix A is not limited to illuminants that can be represented by three linear basis functions.

Still further analyses showed that the high accuracy of the approximation for random illuminants is also not limited to the sensitivities of the cones and to the Munsell reflectances used here. When using random-spline illuminants instead of natural illuminants with the artificial sensors and the artificial reflectances introduced in the two sections below, the linear approximation also explained between 97.7% and 100% and between 97.3% and 99.6% of the variance of the reflected signal depending on the type of sensors and the type of reflectances, respectively. Hence, the linear approximation seems to be very accurate for a large range of illuminants, sensors, and reflectances.

Moreover, the transformation matrices obtained with the different kinds of illuminants were very similar to one another. Further analyses showed that the transformation matrices of one class of illuminants could be used to approximate with high accuracy the reflected signal of Munsell chips under another class of illuminants. The transformation matrices obtained with any of the four kinds of illuminations approximated the reflected signal of the other illuminants on average between 88.4% and 99.7% of the variance, respectively (cf. Supplementary Table S1).

Singularity patterns

The contour plots in the last row of Figure 6 illustrate the singularity index for the Munsell chips calculated with the natural illuminants (panel m), the fluorescent illuminants (panel n), the random-spline illuminants (panel o), and the monochromatic illuminants (panel p). As with natural illuminants (panel m), the local peaks of the singularity index contours for the fluorescent (panel n), random-spline (panel o), and monochromatic (panel p) illuminants were close to unique red, yellow, and green (black circles), and
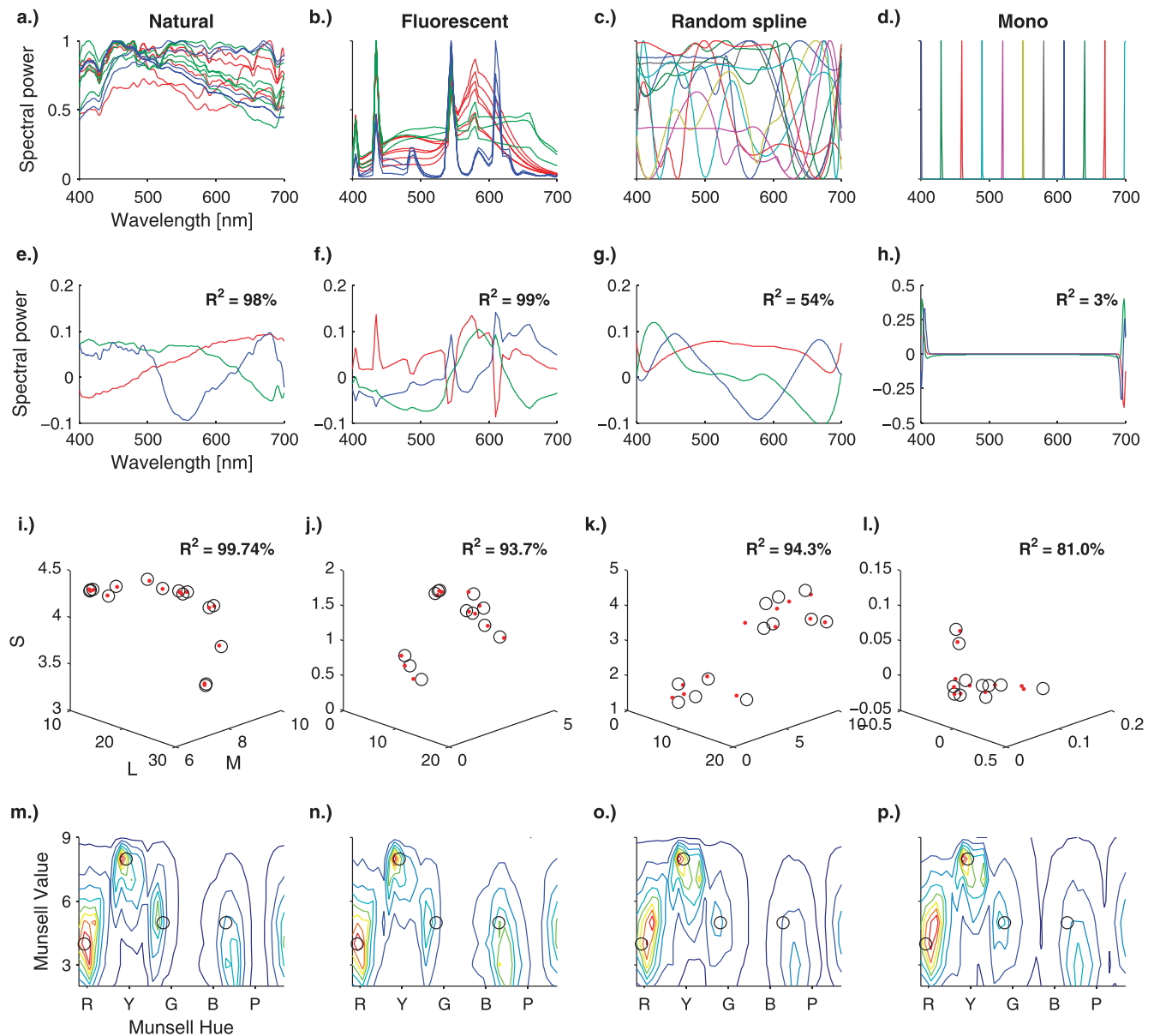
Figure 6. Illuminants. The four columns in this figure correspond to the four kinds of illuminants: natural (first column), fluorescent (second), random spline (third), and monochromatic (last column). The *x*- and *y*-axes in the first (panels a through d) and second (panels e through h) rows correspond to wavelength (in nm) and relative spectral power, respectively. Panel a illustrates examples of daylight illuminants, with red, green, and blue curves corresponding to five examples from the Grenada database (Romero et al., 1997), the Maryland forest illuminants (Chiao et al., 2000), and the simulated daylight spectra (Judd et al., 1964), respectively. Panel b shows the 12 illuminants F, where the red curves correspond to the semibroadbent illuminants F1 through F6, the green curves correspond to the broadbent illuminants F7 through F9, and the blue curves correspond to the narrow triband illuminants F10 through F12. Panels c and d illustrate 12 examples of random-spline and monochromatic spectra, respectively. The three curves in the graphs of the second row (panels e through h) show the first three principal components of the illuminants (red = first component, blue = third component). The principal components were calculated for the complete set of each kind of illuminants (i.e., not only for the few examples shown in the first row). The R^2 in the top right corner indicates how much of the variance of the spectra the first three principal components explain. The third row (panels i through l) illustrates the differences between the reflected LMS signal when calculated with the exact formula (black circles) and when approximated based on the respective matrix A (red dots). The format in this row is the same as that in Figure 1a. As an example, the reflectance of Figure 3a was used, and the reflected signal for the sample illuminants in the first row of this figure (panels a through d, respectively) are shown here. The R^2 in the top right corner indicates how much of the variance of the reflected signal for this reflectance and the respective set of illuminants is explained by the approximation (the average across all reflectances is given in the text). The last row (panels m through p) illustrates the singularity

$\rightarrow$

←

indices across Munsell chips for the different types of illuminants. The format of the panels in this row is the same as that in Figure 4c. For comparison, panel m shows again the singularity indices for the natural illuminants as in Figure 4c. Panels n through p show those for the fluorescent, random-spline, and monochromatic illuminants, respectively. Although the spectra differ strongly across the four sets of illuminants (first row), and although random-spline and monochromatic spectra cannot be represented by three principal components (second row), the linear approximation is extremely accurate for all four types of illuminants (third row), and the patterns of singularities are very similar between these sets of illuminants (fourth row).

---

unique blue was located within contours of relatively high singularity indices.

This was also the case for the evenly sampled sparse set of monochromatic illuminants (Figure 7e). For the center-sampled set, this was the case for red, yellow, and blue but not for green (Figure 7g). However, for left- and right-sampled sets, unique hues did not coincide with peaks of singularities (Figure 7f, h).

Figure 8 illustrates the common variance of the different singularity patterns and the singularity patterns calculated with the natural illuminants (panel a) and with the pattern of focal color choices (panel b). Supplementary Table S2 provides the corresponding statistical details.

The singularity indices for natural illuminants were highly correlated with those of fluorescent ($r = 0.95$, $p < 0.001$), random-spline ($r = 0.91$, $p < 0.001$), and monochromatic ($r = 0.92$, $p < 0.001$) illuminants and the evenly sampled sparse set ($r = 0.93$, $p < 0.001$). These correlations explained significantly more than 50% of common variance (all $p < 0.001$). They imply that those artificial illuminants produced singularities that were highly similar to those of natural illuminants. As a result, the singularities calculated for the transformations under fluorescent, random-spline, monochromatic, and evenly sampled sparse illuminants also explained 40% ($r = 0.64$), 32% ($r = 0.57$), 34% ($r = 0.58$), and 34% ($r = 0.59$) of the variance of focality, respectively (all $p < 0.001$). These correlations do not significantly differ from those based on the natural illuminants and are significantly higher than 20.4% of explained variance, as defined by the 50% criterion. According to these results, the relationship between singularities, focal colors, and unique hues occurs with all those sets of illuminants.

In contrast, the pattern of singularities was significantly altered when illuminants were exclusively sampled from small parts of the visible spectrum, as was the case for the left-, center-, and right-sampled sparse sets of illuminants. Although, the singularities of the center-sampled illuminants still yielded significant correlations with the singularities of the natural illuminants ($r = 0.60$, $p < 0.001$) and with focality ($r = 0.35$, $p < 0.001$), the correlation with the singularities of the natural illuminants explained less than 50% of the variance (37%; $z = -2.3$, $p = 0.02$), and the correlation
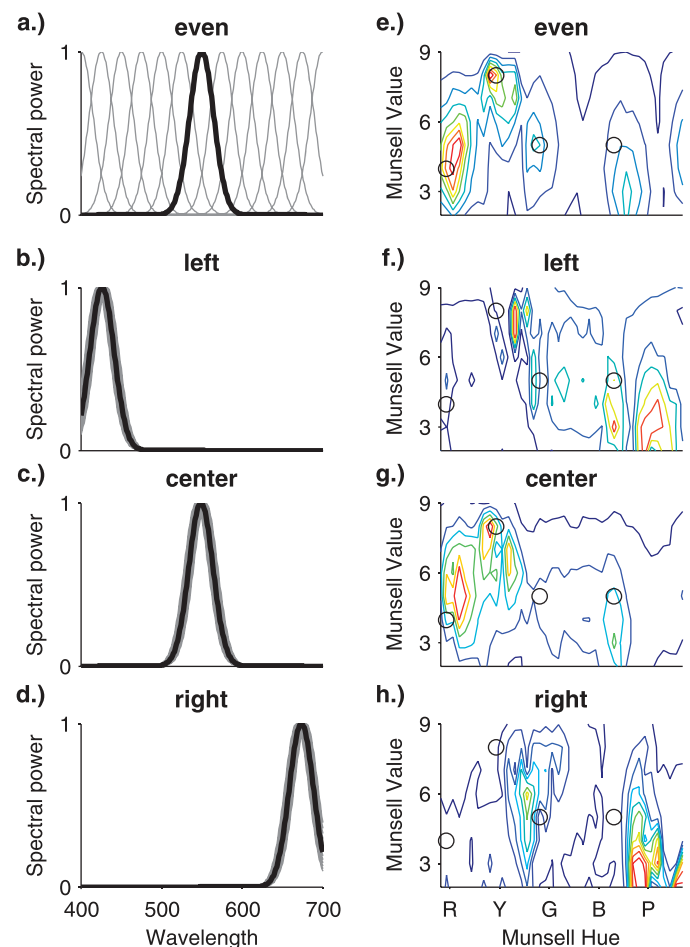

Figure 7. Sparse samples of monochromatic illuminants. Each sample of illuminants consists of 13 Gaussian functions sampled from different regions of the visible spectrum. Those in panel a are sampled evenly at equal wavelength distances across the whole range of the visible spectrum. Those in panels b, c, and d are sampled from the short- (left), medium- (center), and long- (right) wavelength part of the visible spectrum. The panels on the right side (panels e through h) illustrate the corresponding singularity indices. The format is the same as that of the first and last rows of Figure 6. Note that the pattern of singularities changes only when illuminants are not distributed across the whole range of the visible spectrum (panels b through d).
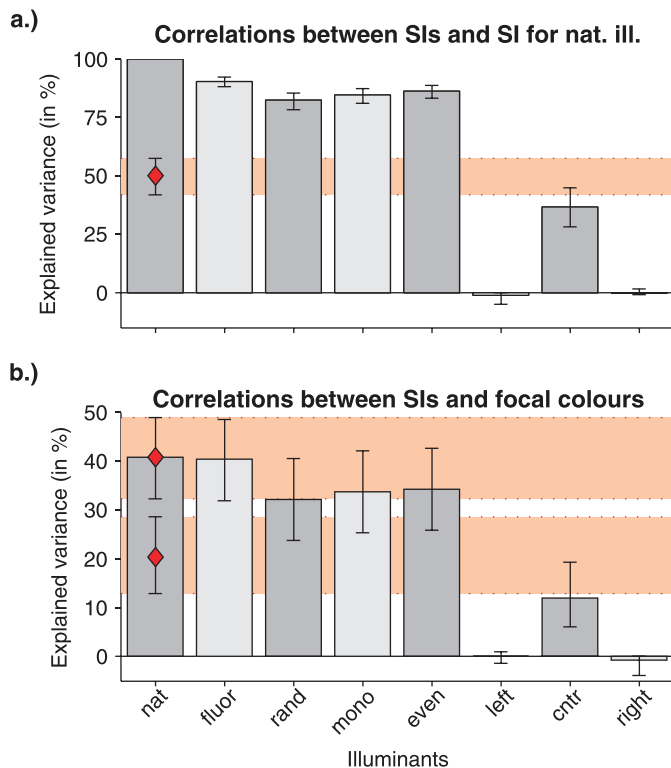
Figure 8. Explained variance across illuminants. The *x*-axis in both panels corresponds to a type of illuminant, where nat = natural, fluor = fluorescent, rand = random-spline, and mono = monochromatic. The rightmost bars correspond to the sparse samples of illuminants, where even = evenly sampled across the whole visual spectrum, left = left- or short-wavelength sampled, cntr = center- or medium-wavelength sampled, and right = right- or long-wavelength sampled. The *y*-axis corresponds to the variance explained by the respective correlation in percentages. Panel a illustrates correlations between the singularity indices calculated with the natural illuminants used in the original studies and those calculated with the illuminants used here. Panel b represents the correlations between the singularity indices and focality (Figure 4b). Error bars show 95% confidence intervals. The first bar (nat) refers to the original settings. The red diamonds refer to 100% and 50% of the respective first bar, and the red bands illustrate the corresponding confidence intervals (based on Fisher transforms). They serve as points of reference for judging the size of the other bars. Note that the first five bars are significantly higher than the 50% criterion (lower red diamond) in both panels, indicating that the singularities based on artificial illuminants produced results similar to those based on natural illuminants; sampling from only a limited region of the visual spectrum strongly changed the results (last three bars).

with focality was significantly lower than the one obtained with natural illuminants (12%; $z = -5.0$, $p < 0.001$). These results indicate that the pattern of singularities and its relationship to focal colors are less reliable when illuminants are sampled only from the

medium-wavelength part of the visible spectrum. However, a weak relationship to focal colors persists.

For the left- and right-sampled sparse sets of illuminants, singularities were positively correlated with neither the singularities of the natural illuminants ($r = -0.11$, $p < 0.04$ and $r = 0.02$, $p = 0.74$, respectively) nor focality ($r = -0.01$, $p = 0.85$ and $r = -0.09$, $p = 0.11$, respectively). All these correlations were significantly below the 50% criterion (all $p < 0.001$). These results show that the pattern of singularities is strongly affected when illuminants are sampled from only one or the other end of the visible spectrum. In this case, the relationship between singularities, focal colors, and unique hues breaks down completely.

Discussion

We observed that the linear approximation of the reflected LMS signal is extremely accurate for all sets of illuminants examined here. Natural, fluorescent, random-spline, and monochromatic illuminants resulted in highly similar transformation matrices. For this reason, it is not surprising that all these sets of illuminants also produced highly similar patterns of singularities across Munsell chips.

The observation that fluorescent, random-spline, and monochromatic illuminations produced transformation matrices and singularity patterns that were similar to the ones found with natural illuminants shows that the transformation of the illuminant into the reflected LMS signal is stable across a wide range of illuminations. On the one hand, the results with fluorescent and monochromatic illuminants (Figure 6b, d) highlight that the pattern of singularities also occurs for peaky, narrow-band illuminants. On the other hand, the results with random-spline and monochromatic illuminants (Figure 6c, d) demonstrate that the pattern of singularities holds for a large range of different illuminants that cannot be represented by three basis functions.

Moreover, the 12 fluorescent and the 13 evenly sampled sparse illuminants produced highly similar patterns of singularity compared with the 300 natural, random-spline, and monochromatic illuminants. This finding demonstrates that the pattern of singularities and its relationship to focal colors does not depend on a large sample of illuminants but may also be produced with a sample as small as 12 illuminants.

We conducted further analyses to examine the role of the shape and the bandwidth of the illuminants. Results are provided in the Supplementary illuminants section of the supplementary materials. Supplementary Figure S6 provides results for spectra with different numbers of random peaks and with shapes that are either smooth or zigzag. Supplementary Figure S7 explores

the role of the bandwidth (i.e., standard deviations) and the shape (i.e., Gaussian, step, or triangular) of monochromatic illuminants. However, none of these properties of illuminants affected the pattern of singularities.

According to our results, the only aspect of the illuminants that strongly affects the pattern of singularities and its relationship to focal colors and unique hues is the range of the visible spectrum from which illuminants are sampled. In particular, when illuminants are sampled exclusively from one or the other end of the visible spectrum, the pattern of singularities is strongly altered and the relationship to focal colors breaks down. Taken together, these results suggest that the pattern of singularities across colors does not depend strongly on the type of illumination as long as illuminants are sampled across the whole range of the visible spectrum.

Sensors

The sensitivities of the human photoreceptors, the cones, may be mathematically represented by color-matching functions for arbitrary, virtual sensors (e.g., RGB), tristimulus values (XYZ), and cone fundamentals (LMS). The singularity index is invariant as to this kind of representation and as to the relative scaling of the sensitivities. This is illustrated by Supplementary Figure S8 in the Different measurements of cone sensitivities section of the supplementary materials. For this reason, here we concentrate on the results with the cone sensitivities of Stockman and Sharpe (2000).

Koenderink (2010) argued that the characteristics of the cone sensitivities may be at the source of invariances in the distribution of color signals. Figure 9a shows the sensitivity spectra of the cones according to Stockman and Sharpe (2000). The sensitivity spectra of the cones have a particular shape that is almost, but not exactly, Gaussian. They are asymmetrically arranged across the visible spectrum. Moreover, the sensitivity spectra of the M- and L-cones (green and red curves, respectively, in Figure 9a) strongly overlap, resulting in high correlations between M- and L-cone excitations (cf. Figure 1). These particularities of the human photoreceptors may be at the source of the irregular distribution of the singularity indices across colors (Figure 4c). We tested this idea by using a large range of artificial sensors.

In preliminary investigations, we produced artificial sensors based on random Gaussian and random-spline distributions (cf. Witzel et al., 2014). The results suggested that the distributions of the singularity index are comparatively stable across different locations of the sensitivity spectra within the visible spectrum,

different degrees of overlap and correlation between the sensors, and different shapes of the sensitivity spectra. What had the largest impact on the pattern of singularity indices was whether the sensors covered the whole visible spectrum or only parts of it. Here, we systematically varied the location, the overlap and correlation, the shape, the width, and the overall range of the sensitivity spectra to test these preliminary findings.

Method

To examine the impact of the location of the sensitivities along the spectra, we produced inverted spectra (Figure 9b). Inverted spectra consist of the cone fundamentals mirrored horizontally along the visible spectrum (400–700 nm). Consequently, these sensors have a similar shape as human cones but the inverse location.

To check whether the correlations between the spectral sensitivities affect the singularity index, we produced three equally spaced spectral sensitivities that did not overlap (Figure 9c) and three that strongly overlapped (Figure 9d). The former set of sensors consisted of three normal distributions that were distanced by 6 *SD*, with less than 0.3% overlap, and the overlapping 0.3% was set to zero. For the strongly overlapping set of sensors the Gaussians were only 1 *SD* away from each other, which corresponds to 61.7% overlap, and the overlapping parts were not set to zero.

To examine the impact of the shape of the excitation spectra, we produced linear (Figure 9e), sigmoidal (Figure 9f), and two kinds of sinusoidal sensors (Figure 9g, h). The three linear sensors increased linearly from the center toward one end and the other end of the visible spectrum and from the two ends of the spectrum toward the center, respectively. The sigmoidal sensors were produced through a logistic regression based on a binomial distribution so that the sensors converged toward 0 and 1 at one end and the other end of the visible spectrum, respectively. Two of the sensors were at 0.5 in the center of the visible spectrum (red and blue curves, respectively, in Figure 9f), and the third was shifted toward shorter wavelengths (green curve). The first set of sinusoidal sensors was symmetrical. It was produced by three sine functions for which one cycle ($2*\pi$) was equal to the visible gamut and that were shifted by 90° ($\pi/2$) away from each other (Figure 9g). The second set of sinusoidal sensors was asymmetrical because it included one sensor (green curve) that was shifted by only 18° ($0.1*\pi$) away from the short-wavelength sinusoidal sensor.

To assess the impact of the bandwidth of the sensors, we produced narrow-band (Figure 9i) and broad-band
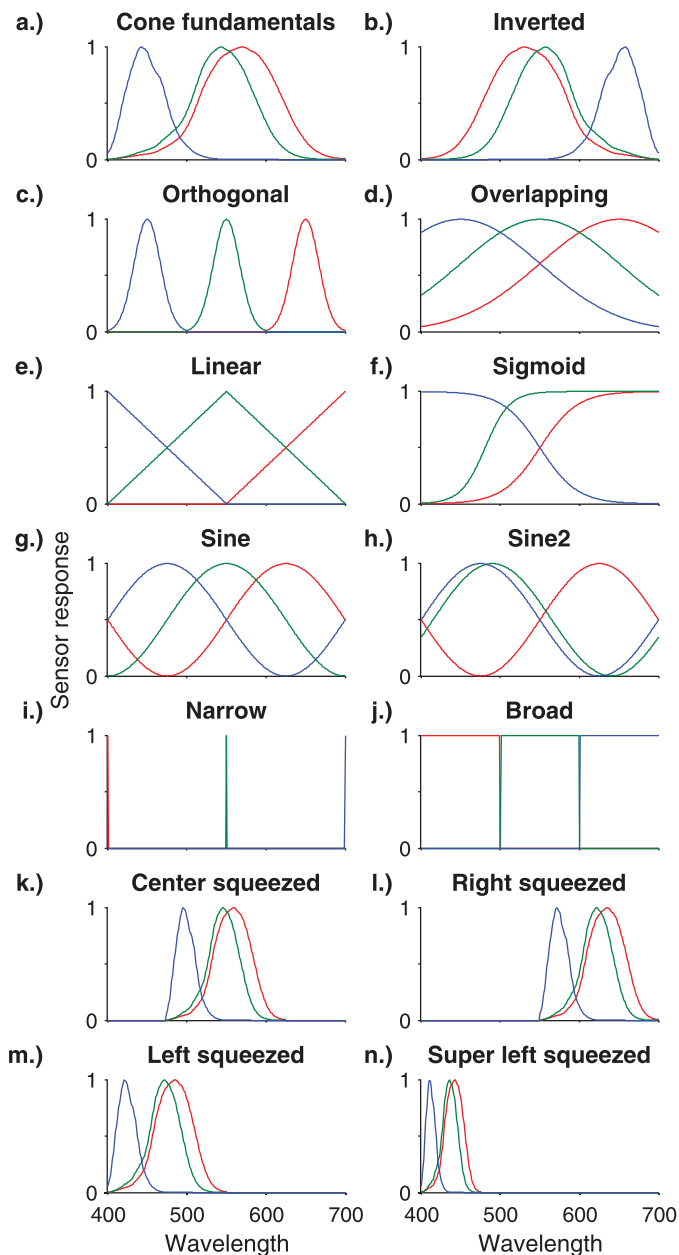
Figure 9. Real and artificial sensors. Panel a shows the cone fundamentals of Stockman and Sharpe (2000), and panel b horizontally mirrored ("inverse") cone fundamentals. Panels c through j illustrate the following sensors: (c) nonoverlapping orthogonal, (d) strongly overlapping Gaussian, (e and f) linear and sigmoidal, (g and h) sinusoidal, and (i and j) narrow band and broad band. The sensors in panels k through n have the same shape as cone fundamentals, but their range of wavelength sensitivity is squeezed around the center (panel k) toward the longest (panel l) and toward the shortest wavelength (panels m and n). The squeezed sensors (panels k through m) are squeezed by a factor of 2, and the super-squeezed sensors (panel n) are squeezed by a factor of 4. Note that spectra differ in location, overlap (correlation), shape, bandwidth, and the range of the visible spectrum across which they are distributed.
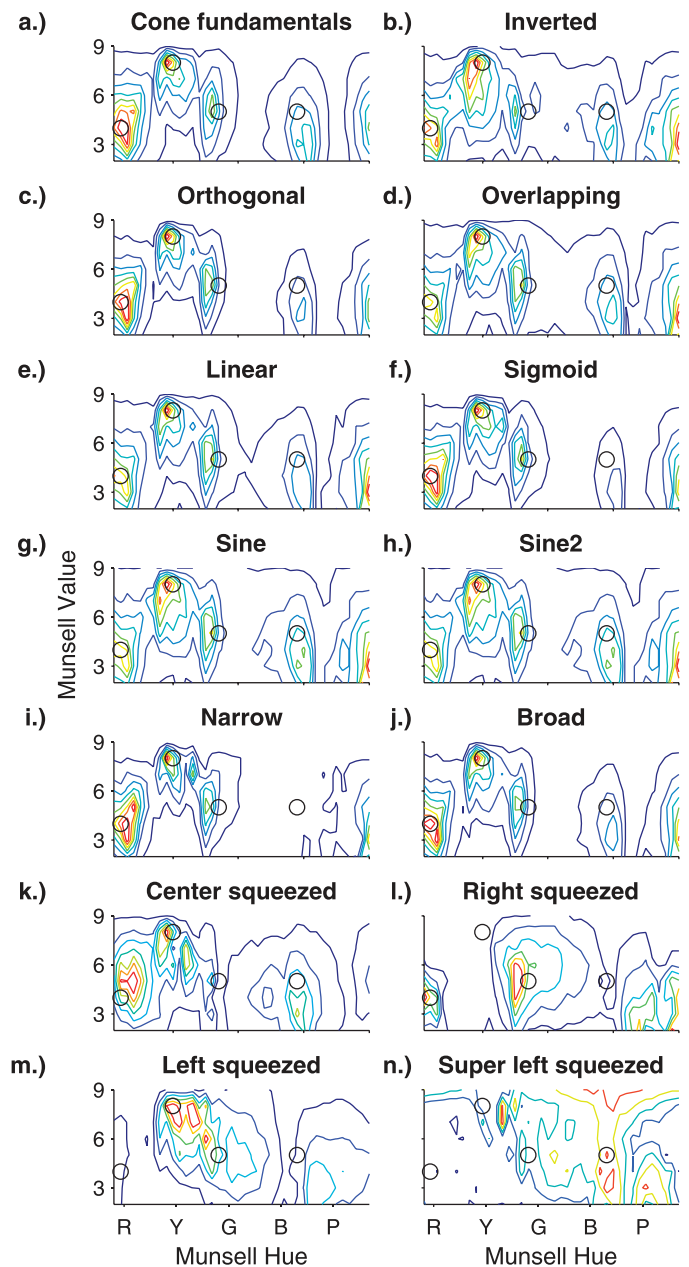

Figure 10. Singularity indices for different sensors. Panels correspond to the sensors shown in Figure 9. The format is the same as that in Figure 4c. Note that the distribution of singularities is robust across variations in the location, overlap, shape, and bandwidth of the sensitivity spectra (panels b through j) and is most strongly affected by reducing ("squeezing") the visible spectrum (panels k through n).

(Figure 9j) sensors based on step functions, which are either on (1 = *maximal excitation*) or off (0 = *minimal excitation*). Narrow-band sensors consisted of three sensors that were on at 400, 550, and 700 nm, respectively, and off for the rest of the visible spectrum. Broad-band sensors were on for 400 to 500, 500 to 600, and 600 to 700 nm, respectively.

Finally, we produced four sets of squeezed sensors that did not range over the whole visible spectrum (Figure 9k through n). For three of the sets, we reduced the spectral range of the cone fundamentals to half of the original range. The first set was located around the center of the visible spectrum (cf. "center squeezed" in Figure 9k), the second set was located at the long-wavelength end (cf. "right squeezed" in Figure 9l), and the third set was located at the short-wavelength end of the visible spectrum (cf. "left squeezed" in Figure 9m). The fourth set consisted of super left-squeezed sensors. The range of these sensors was reduced to one fourth of the original range, and the sensors were located at the short-wavelength end of the spectrum (Figure 9n).

To test the impact of the sensors on the singularity index, the same natural illuminations and Munsell chips used in Philipona and O'Regan (2006) were used as illuminants and reflectances. However, singularity patterns and their relationship to focal colors could be affected by a combined effect of changes to the sensors and changes to the illuminants. In order to examine such interaction effects, we also inspected singularity patterns for the different sensors under fluorescent (cf. Figure 6b), random-spline (cf. Figure 6c), and mono-chromatic (cf. Figure 6d) illuminants.

Results

Effects of sensors under natural illuminants

Figure 10b through n shows the distribution of the singularity index when using artificial sensors. Apart from the super-squeezed sensors (Figure 10n), unique yellow (second black circle from left) was close to peaks in singularity indices for all sensors. For unique red (leftmost black circle), this was the case for all but the two left-squeezed sensors (Figure 10m, n). In most cases, unique green (third circle from left) and blue (fourth circle from left) were also close to peaks of singularity indices. However, unique green did not coincide with peaks of singularities for inverted (Figure 10b), center-squeezed (Figure 10k), and super-squeezed (Figure 10n) sensors. Unique blue was not located close to the peaks for the narrow-band (Figure 10i), right-squeezed (Figure 10l), and left-squeezed (Figure 10m) sensors.

Figure 11 illustrates the variance explained by the correlations between the singularity indices for the different sensors and those for the cone fundamentals (Figure 11a) and between singularity indices and focal color choices (Figure 11b). Dark bars correspond to the left panels of Figure 10, and light bars correspond to the right panels of Figure 10. Supplementary Table S3 provides the corresponding statistical details.

Apart from the super-squeezed sensors, the singularity indices for all sensors were positively and highly significantly correlated with those for the human cones

(all $p < 0.0001$) and were highly significantly correlated to focality (maximum $p = 0.005$). Based on the criteria for comparing correlations, three main groups of sensors may be distinguished.

The first group consists of sensors that produced highly similar singularity indices as cone fundamentals (cf. Figure 10a). This group included orthogonal, nonoverlapping (Figures 9c and 10c), overlapping (Figures 9d and 10d), linear (Figures 9e and 10e), sigmoidal (Figures 9f and 10f), sinusoidal (Figures 9g, h and 10g, h), and broad- and narrow-band (Figures 9i, j and 10i, j) sensors. The correlations between the singularities of these sensors and those obtained with cone sensitivities shared significantly more than 50% of the variance, with correlation coefficients varying between $r = 0.84$ and $r = 0.96$ (cf. Figure 11a). Among those sensors, orthogonal, linear, sigmoid, and broad-band sensors yielded correlations with focality that explained significantly more (all $p < 0.05$; cf. Supplementary Table S3) than 50% of the variance explained through the correlations based on cone sensitivities (cf. Figure 11b).

The second group consisted of sensors whose pattern of singularities strongly differed from the one obtained with cone sensitivities. This group included right-squeezed (Figure 9l and Figure 10l), left-squeezed (Figures 9m and 10m), and super left-squeezed (Figures 9n and 10n) sensors. The correlations between the singularities of these sensors and those of the cones explained significantly less than 50% of the variance, with correlation coefficients varying between $r = -0.26$ and $r = 0.25$ (Figure 11a). Their correlations with focality were significantly below the 50% criterion (all $p < 0.001$; cf. Figure 11b).

Finally, results for the two remaining sensors—the inverted and the center-squeezed sensors—showed weak effects on the pattern of singularities and their relationship to focal colors (Figure 9b, k and Figure 10b, k). The correlations of the singularities with those for the cone sensitivities ($r = 0.76$ and 0.73, respectively) did not explain significantly more than 50% of the variance (cf. Figure 11a), and at the same time the correlations with focality were significantly smaller than those obtained with the cone sensitivities (cf. Figure 11b). Nevertheless, both kinds of correlations were not significantly below the 50% criterion (cf. Figure 11a, b).

Taken together, only squeezed and inverted sensors affected the pattern of singularities and their relationship to focal colors considerably. These results highlight that the range of the sensitivity spectrum and the location of the sensors play a considerable role for the pattern of singularities. This observation is in line with those found with random-normal and random-spline spectra in the preliminary study (Witzel et al., 2014). We provide supplementary results with those random
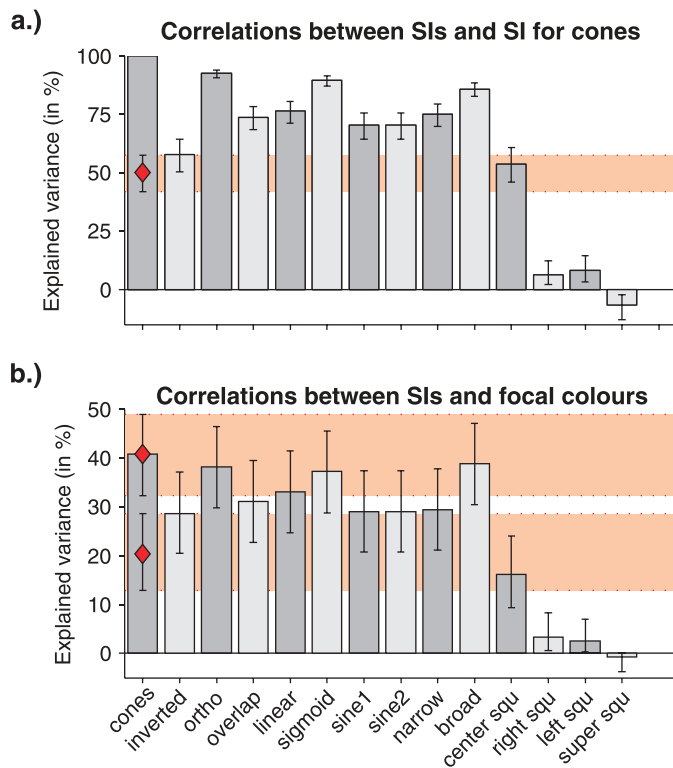
Figure 11. Explained variance across sensors. Apart from the *x*-axis, the format is the same as that in Figure 8. The *x*-axis corresponds to the different kinds of sensors. Most sensors resulted in correlations above the 50% criterion; only the squeezed sensors produced correlations below the 50% criterion.

sensors in the Random sensors section (Supplementary Figures S9 and S10 and Supplementary Table S4) of the supplementary materials.

Effects of sensors under artificial illuminants

The Interaction effects between sensors and illuminants section of the supplementary materials provides detailed results on the effects of varying sensors under fluorescent, random-spline, and monochromatic illuminants (Supplementary Figure S11 and Supplementary Tables S5 and S6). In sum, results obtained with fluorescent, random-spline, and monochromatic illuminants were similar to those obtained above with natural illuminants. For all types of illuminants, singularities for all sensors were significantly positively correlated with the singularities obtained with the cone sensitivities under natural illuminants and with focality (all $p > 0.05$). The only exceptions were again the super left-squeezed sensors. Moreover, under random-spline and monochromatic illuminants, the correlation with focality was only marginally significant ($p < 0.1$) for the left-squeezed sensors.

With respect to the size of these correlations, random-spline and monochromatic illuminants yielded correlations that were similar to those of natural illuminants (cf. Supplementary Figure S11c through f). In contrast, fluorescent lights had a stronger effect on the singularity pattern for some of the sensors (cf. Supplementary Figure S11a, b). In particular, the singularity pattern produced with sine-wave and center-squeezed sensors yielded correlations below the 50% criterion. This was due to the fact that under fluorescent illuminants the peak of singularities around focal and unique yellow, red, and green was strongly reduced.

The correlations above indicate that differences between the illuminants have stronger effects on singularities for some sensors than for others. To further clarify this interaction between sensors and illuminants, we inspected the effect of illuminants on singularities for each kind of sensor separately. For this purpose, for each sensor we calculated correlations between singularities obtained under natural illuminants and those obtained under fluorescent, random-spline, and monochromatic illuminants. These correlations are provided in Supplementary Table S7. All of these correlations were significant. Random-spline and monochromatic illuminants produced very similar patterns of singularities compared with natural illuminants for all sensors, with a minimum correlation of $r = 0.90$ (82%) for sigmoid sensors. In contrast, correlations varied much more across sensors when using fluorescent illuminants, for which lowest correlations were only $r = 0.73$ (54%) for the two sinusoidal sensors and $r = 0.79$ (63%) for the super left-squeezed sensors. Singularities of narrow-band sensors did not change across illuminants at all (all $r = 1$). These correlations suggest that, when considering artificial sensors, fluorescent illuminants had a stronger effect on singularity patterns and that these effects were different for different sensors.

In sum, the effects of sensors and illuminants combine in the case of certain sensors and fluorescent illuminants. However, for random-spline and monochromatic illuminants, the effects of sensors remained largely the same as under natural illuminants.

Discussion

Singularities were surprisingly stable across different sensors. Apart from squeezing and inverting the sensors, changes to the characteristics of the sensors did not fundamentally change the pattern of the singularities and their relationship to focal colors and unique hues.

For certain sensors, changing illuminants from natural to fluorescent affected the singularity pattern.

Because fluorescent illuminants are more narrow band and peaky, the small set of these illuminants selectively samples only parts of the reflectance spectrum when being reflected off a surface. In this case, the LMS signal depends more strongly on which parts of the spectrum are sampled by the different kinds of sensors. Consequently, some of the sensors may miss characteristics in the variation of the LMS signal under fluorescent illuminants that they would have captured under natural and random-spline illuminants. However, even in this case the relationship between singularities and focal colors persists across the different sensors as long as their sensitivities are not strongly squeezed.

The present results allow the evaluation of the impact of the symmetrical arrangement of sensitivities across the visible spectrum, their shape, their degree of overlap, their bandwidth, their location within the visible spectrum, and the range of the visible spectrum across which sensitivity spectra are distributed. First, in contrast to human cones, Gaussian (Figure 9c, d), linear (Figure 9e), the first set of sinusoidal (Figure 9g), and the step (Figure 9i, j) functions were symmetrical to the center of the visible spectrum (550 nm). Nevertheless, they produced similar singularity indices compared with the human cones. Consequently, the asymmetry of the human sensitivity spectra is not at the source of the irregular distribution of singularity indices across Munsell chips and their relationship to focal colors and unique hues.

Second, linear (Figure 9e), sigmoidal (Figure 9f), sinusoidal (Figure 9g, h), and step (Figure 9i, j) functions strongly differed from the sensitivity spectra of human photoreceptors in their shape. Nevertheless, they yielded highly similar singularity indices, which coincided with focal colors and unique hues. These results show that the shape of the sensitivity functions does not play a major role in the distribution of singularities and their relationship to focal colors and unique hues.

Third, singularity indices barely changed when using orthogonal sensors instead of cones. This observation shows that the correlation of L- and M-cones (red and green curves, respectively, in Figure 9c) does not determine the distribution of singularities and their relationship to focal colors. At the same time, overlapping Gaussian (Figure 9d), linear (Figure 9e), sigmoidal (Figure 9f), and sinusoidal (Figure 9g, h) sensors strongly overlapped. Nevertheless, these sensors yielded similar singularities compared with the human cones. These results show that the overlaps among spectral sensitivities, and the resulting correlations among the color signals, are largely irrelevant for the distribution of the singularity index across colors and their relationship to focal colors and unique hues.

Fourth, narrow-step (Figure 9i), orthogonal (Figure 9c), broad-step (Figure 9j), and overlapping (Figure 9d) sensors have increasing degrees of bandwidth. However, the fact that they yielded similar singularities compared with the human cones indicates that the bandwidth is not a major factor either.

Fifth, the inverted spectra (Figure 9b) had a similar shape compared with the human cones but differed mainly by their location along the spectrum. This shift in location affected singularities, but only moderately. Other unsqueezed spectra, such as the orthogonal and sigmoidal sensors (Figure 9c, f), were also located at different points along the spectrum compared with the human cones. The fact that they yielded extremely similar singularities (95% and 96%, respectively) as the cones indicates that it is not location alone that shapes the pattern of singularities.

Finally, squeezing the range of sensitivities reduced (simply squeezed) and even inverted (super squeezed) the correlation of the corresponding singularity indices compared with that of the cones (Figure 9k through n). Strongly squeezing the spectra also destroys the relationship between singularities and focal colors and unique hues, as shown by the super-squeezed sensors (Figures 9n and 10n). However, the comparison between left-, center-, and right-squeezed sensors revealed that the squeezing effect was also modulated by the location of the sensors along the visible spectrum.

In sum, these observations suggest that the main characteristic of the sensors that matters for the relationship between singularities, focal colors, and unique hues is whether their spectra are distributed over the whole visible spectrum. This effect is modulated by the location of the sensors along the visible spectrum. However, as long as the range of sensitivities of the sensors extends to both ends of the visible spectrum, major characteristics of the sensors, such as the amount of overlap and the shape of the sensitivity functions, do not disrupt the relationship between singularities on the one hand and focal colors and unique hues on the other. This conclusion is further supported by our previous results with random-normal and random-spline sensors (Witzel et al., 2014).

Surfaces

There are two critical questions concerning the characteristics of the maximally saturated Munsell chips used by Philipona and O'Regan (2006) to establish a relationship with focal colors. First, these Munsell chips had different Munsell chroma because the Munsell system does not provide the same range of Munsell chroma for all levels of hue and lightness. As

shown by Figure 5b, the singularity index correlates more strongly with Munsell chroma ($r = 0.70$, 49%, $p < 0.001$) than with focal color choices ($r = 0.64$, $p < 0.001$; see also Supplementary Figure S5b, d). At the same time, it has been observed that focal color choices also coincide with some of the most saturated Munsell chips (Collier, 1973; Munsell, 1912; Regier et al., 2007; Witzel & Franklin, 2014). As shown by Figure 5c, focal color choices correlate with Munsell chroma ($r = 0.41$, 17%, $p < 0.001$). With respect to those correlations, the question arises of whether the pattern of singularities across Munsell hue and value depends on differences in Munsell chroma and whether the relationship between singularity index and focal colors is due to these differences in Munsell chroma. To some extent this question may be answered by calculating the partial correlation between singularities and focal color choices, controlling for Munsell chroma. This partial correlation ($r = 0.54$, 29%, $p < 0.001$) supports a relationship between singularities and focal colors independent of Munsell chroma. Consequently, singularities should be correlated with focal colors even when Munsell chroma is constant. To test this idea, we examined Munsell chips that are more uniform in Munsell chroma.

Second, Munsell chips are made of particular artificial pigments (Munsell, 1912). For this reason, they may have particular reflectance properties that are different from those of other surfaces. For example, reflectances of the sample of Munsell chips used here can be linearly decomposed into three basis functions, as illustrated by Supplementary Figure S12a and b (see also Cohen, 1964; Maloney, 1986; Romney & Indow, 2003; but see Parkkinen et al., 1989). The question arises of whether the pattern of singularities that is related to focal colors and unique hues depends on the particular spectral composition of Munsell chip reflectances or whether surfaces that look the same or at least highly similar under the most common illuminations produce similar singularities as Munsell chips. For example, does a surface with the same red as the perfectly red Munsell chip but with a different reflectance spectrum also have a particularly high singularity? To investigate this question we examined surfaces that produce the same LMS signal as the Munsell chips when they reflect white light. When two lights produce exactly the same LMS signal, they are called *metameric*.

However, due to *metameric mismatching*, surfaces that are metameric under a particular neutral illumination will not be metameric under different illuminations (Logvinenko, Funt, & Godau, 2014; Wyszecki & Stiles, 1982). Hence, sets of metameric reflectances vary depending on the illuminant under which they are metameric matches. At the same time, these surfaces still look similar under a wide range of neutral illuminations. For example, red surfaces that are metameric under daylight would still look red under a tungsten bulb (whether this is due to color constancy or insensitivity to small changes is not of importance here). If high singularity is a general property of reddishness, all red surfaces should have this property independent of the effects of metameric mismatching. Consequently, patterns of singularities should be stable across variations of reflectances that result from metameric mismatching under neutral illuminations. To assess potential effects of these variations, we used two kinds of light—equal-energy light and daylight—to produce artificial surfaces that are metameric with Munsell chips under that light.

Method

To make Munsell chips more uniform in chroma, we had to reduce the Munsell chroma of chips whose maximal chroma was high in order to match the Munsell chroma of the other chips. However, some dark and light Munsell chips (Munsell value = 2 or 9) are available only with a Munsell chroma of 2, and at this level of chroma most colors tend to be called *gray* or *white* (cf. figure 8 in Olkkonen, Witzel, Hansen, & Gegenfurtner, 2010). It would be meaningless to compare such desaturated colors with focal color choices. For this reason, we could not use Munsell chips with equal Munsell chroma across hue and lightness. Hence, we simply replaced all Munsell chips with a Munsell chroma above 6 in the set of maximally saturated Munsell chips with chips with a Munsell chroma equal to 6. Because those particularly light or dark Munsell chips are not available at this Munsell chroma, even our set of Munsell chips with uniform Munsell chroma still involved differences in Munsell chroma across Munsell chips. For the sake of simplicity, we call these chips "uniformly saturated" for now and come back to this issue when discussing the results. Figure 13b illustrates the reflectance spectra of the uniformly saturated Munsell chips that correspond in hue and lightness to the maximally saturated ones in Figure 13a. Note that some spectra are the same in panels a and b because there is no Munsell chroma larger than 6 for those Munsell hues and values.

To obtain sets of reflectances that are metameric with the Munsell chips under neutral illuminations, we determined surface reflectances that produce metameric LMS signals when reflecting equal-energy white or daylight (cf. Figure 12a). For this purpose, we calculated the spectra reflected off the surfaces of the Munsell chips under equal-energy light (CIE standard illuminant E) and simulated daylight (CIE standard illuminant D65).
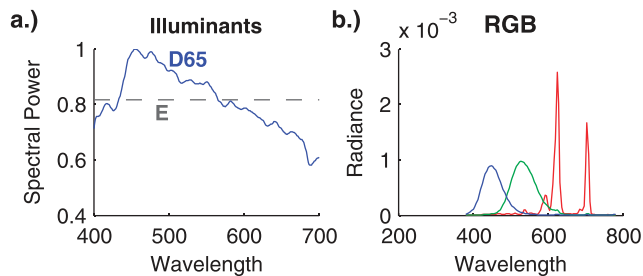
Figure 12. White illuminants and RGB spectra. Panel a shows the relative spectral power distribution for illuminants E (dark gray, dashed curve) and D65 (blue curve). Panel b depicts the radiances measured for the three phosphors (RGB) of a cathode ray tube monitor. These RGB spectra were used to create artificial reflectances that were metameric with Munsell chips under the illuminants of panel a.

We used two approaches to produce surfaces for which the reflected light is metameric with the reflected light of the Munsell chips. First, in the RGB approach, we decomposed the scattered light into linear basis functions that corresponded to the spectra of the RGB primaries of a typical cathode ray tube monitor. The monitor was an Iiyama MA203DT (Iiyama Deutschland GmbH, Ilm, Germany) driven by an NVIDIA graphics card (NVIDIA Corporation, Santa Clara, CA), and the spectra of the monitor primaries were measured with a Photo Research PR650 spectrometer (Photo Research Incorporated, Chatsworth, CA). The resulting spectra are shown in Figure 12b. Second, we calculated the *fundamental metamers* for the spectra of the light reflected off the Munsell chips (Cohen & Kappauf, 1982). A fundamental metamer is the part of the impinging spectrum that is common to all metameric impinging spectra. In both cases we determined the reflectances that would reflect these lights under those illuminants (Burns, Cohen, & Kuznetsov, 1989; Wyszecki, 1958). Note that for illuminant E the profiles of the impinging spectra are the same as those of the reflectances. These two approaches provided us with two sets of artificial surface reflectances for each set of Munsell chips (maximally and uniformly saturated) and each illuminant (E and D65).

Figure 13c through f illustrates the artificial reflectances that are metameric under illuminant E with those in panels a and b. The second row (panels c and d) shows the reflectances produced through the spectra of the RGB primaries, and the third row shows those based on the fundamental metamers under illuminant E. Reflectances that reflect metameric lights under illuminant D65 look similar to those produced through metamers under illuminant E. For this reason, examples of reflectances that are metameric under illuminant D65 are provided in Supplementary Figure S13 rather than in the main article.

Some of the artificial reflectances were partly below 0 or above 1 (Figure 13c through f). Physical reflectance spectra of real surfaces are necessarily positive and not larger than 1 (apart from photoluminescent surfaces). Zero means that they absorb all light, and 1 means that they completely reflect all light. We tried several techniques for creating artificial reflectances. If reflectances were limited to the range between 0 and 1, the LMS signal of maximally saturated Munsell chips could be produced only by reflectances that were highly similar to those of Munsell chips. However, if reflectances are very similar to Munsell chips, they do not allow the testing of the impact of spectral characteristics on the singularity index. For this reason, we used the artificial reflectances based on RGB and fundamental metamers to investigate this question from a theoretical perspective. We come back to this issue in the General discussion.

As before, the set of natural illuminants and the human cone fundamentals were used to calculate LMS signals and singularity indices. We also examined whether changing reflectances and changing illuminants and sensors together produced interaction effects on singularities that could not be predicted by the separate effects of reflectances, sensors, and illuminants.

Results

Figure 14 and Supplementary Figure S14 illustrate the distribution of singularities across Munsell hue and value for the different kinds of reflectances. The panels of these figures correspond to the types of reflectances in Figure 13 and Supplementary Figure S13, respectively. Analogously to Figures 8 and 11, Figure 15 illustrates the results of the main tests in terms of the variance explained by the respective correlations. Figure 15a corresponds to the correlations of the singularities shown in Figure 14 and Supplementary Figure S14 with the singularities obtained with the maximally saturated Munsell chips shown in Figure 14a. Figure 15b illustrates the correlations between singularities and focal color choices. Supplementary Table S8 provides the statistical details on these correlations.

Maximally saturated reflectances

The dark bars in Figure 15 show results with maximally saturated reflectances. Figure 15a suggests that the singularity indices are affected by the type of reflectance. Figure 15b indicates that the strength of the relationship between singularities and focal colors increases with the similarity between the singularity pattern and the one of the maximally saturated Munsell chips, as shown in Figure 15a.
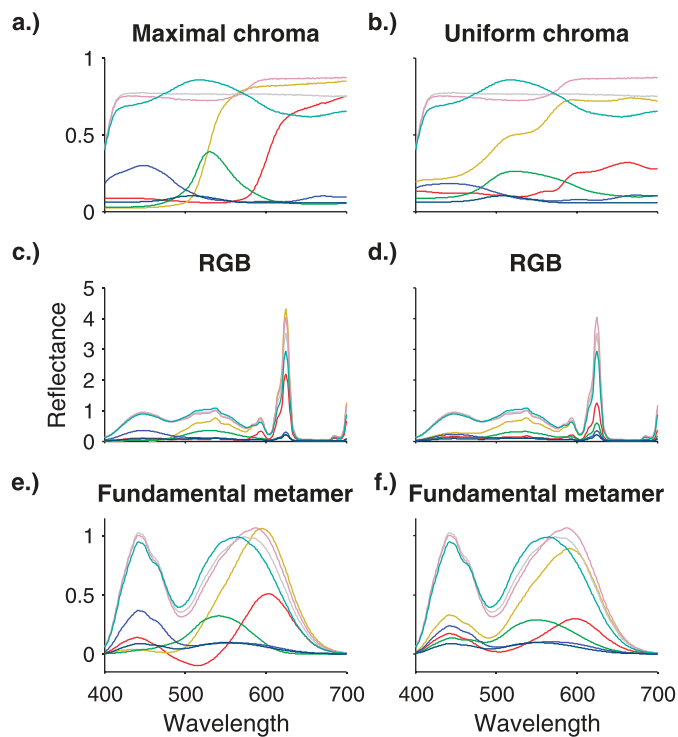
Figure 13. Reflectance spectra for Munsell chips and artificial reflectances. The format is the same as that in Figure 2a through d. Panel a illustrates the spectra of maximally saturated Munsell chips through the nonsingular examples of Figure 2 and the singular examples of Figure 3. Panel b shows the spectra of the uniformly saturated set of Munsell chips that correspond to those in panel a in terms of hue and lightness. Panels c and e on the left side show artificial spectra that are metameric under illuminant E with the maximally saturated Munsell chips in panel a. Panels d and f on the right side show the artificial reflectances that are metameric with the uniformly saturated Munsell chips in panel b. The artificial reflectancs in the second row (panels c and d) were produced with the RGB approach. The artificial reflectances in the third row (panels e and f) were created based on the fundamental metamers. Corresponding reflectances produced when assuming illuminant D65 are provided in Supplementary Figure S13. Note the strong differences between the spectra across the rows. Moreover, some of the artificial reflectances transgress the interval [0, 1], indicating that these reflectances may be used for theoretical explorations only and not for real surfaces (for details see text).

Singularity indices for RGB reflectances ("RGB-max" and "RGB-max D65") shared more than 87% of the variance with those for the maximally saturated Munsell chips ($r = 0.94$ and 0.93, respectively; both $p < 0.001$). Consequently, unique hues (black circles in Figure 14 and Supplementary Figure S14) also coincided with the peaks of singularities, and singularities were highly correlated with focality (both $r = 0.61$, $p < 0.001$). All these correlations were significantly higher than the 50% criterion ($p < 0.01$). These
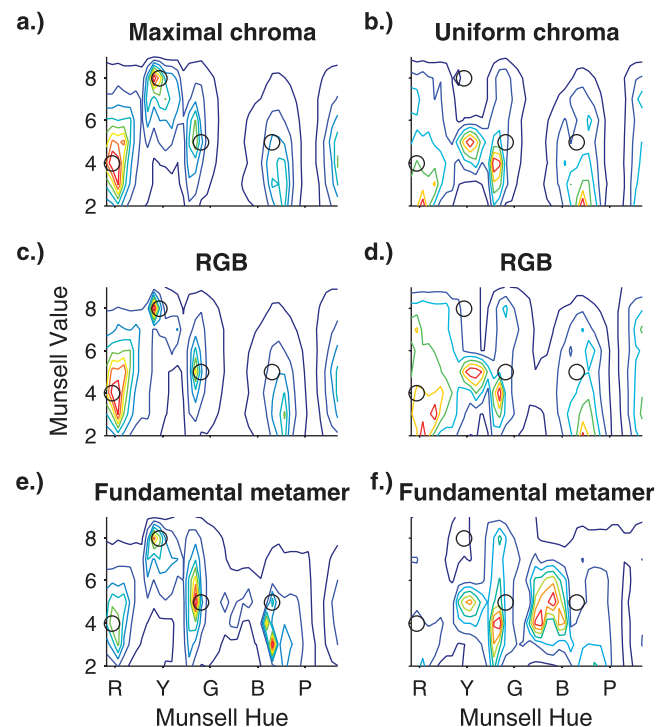
Figure 14. Singularity index for Munsell chips and artificial reflectances. Following the arrangement of Figure 13, the graphics show the singularity indices for the maximally (panel a) and uniformly (panel b) saturated Munsell chips, for the reflectances produced with the RGB approach (panels c and d), and with the fundamental metamer approach (panels e and f) under illuminant E. Singularity indices for reflectances that are metameric with Munsell chips under illumininant D65 are provided in Supplementary Figure S14. Note that uniformly saturated Munsell chips produced different patterns of singularities compared with maximally saturated ones (columns) and that singularities also vary across the different kinds of reflectances (rows).

results show that maximally saturated reflectances based on RGB spectra produced singularities that were highly similar to maximally saturated Munsell chips.

Using fundamental metamers affected the patterns of singularities more strongly, and it made a difference whether metamers were produced under illuminant E ("FM-max") or D65 ("FM-max D65"). Like the maximally saturated Munsell chips (Figure 14a), the singularities for the fundamental metamers of the maximally saturated Munsell chips under illuminant E showed peaks of singularities close to the unique hues (Figure 14e). The correlations of these singularity indices and those of the original chips explained 67% of the variance ($r = 0.82$, $p < 0.001$), which is significantly more than 50% ($z = 3.5$, $p < 0.001$). At the same time, the correlation with focality explained only 30% of the variance ($r = 0.55$, $p < 0.001$), which is marginally different from the 41% found with Munsell chips ($z = -1.7$, $p = 0.08$).
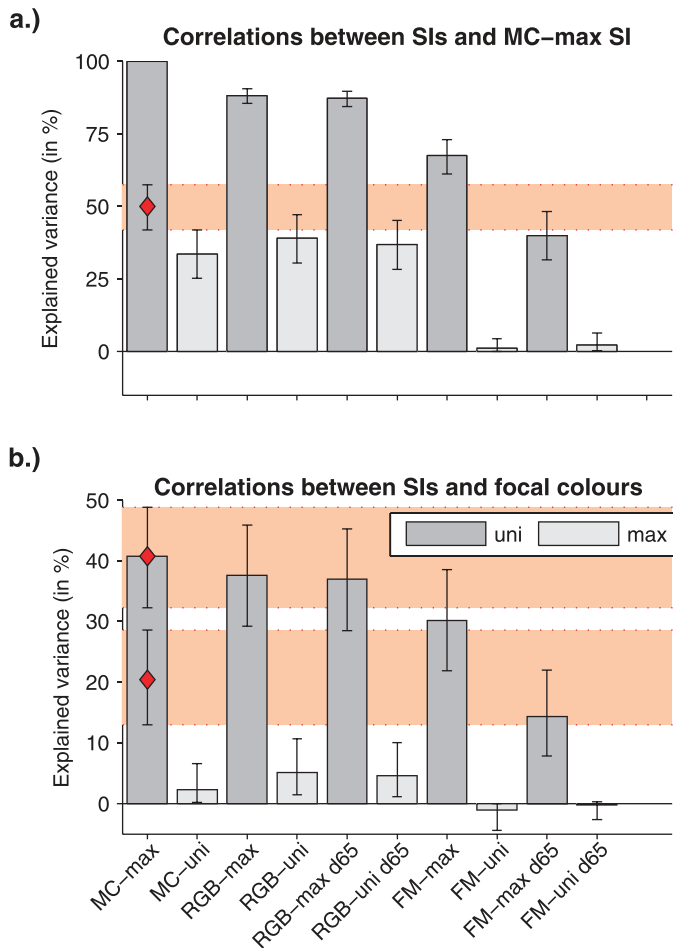
a.)

b.)

Figure 15. Explained variance across reflectances. The *x*-axis refers to the different kinds of reflectances. Apart from that, the format is the same as that in Figures 8 and 11. Note that singularity indices of reflectances with uniform Munsell chroma explain less than 20% of the variance of focal color choices.

The singularities for the fundamental metamers under D65 were still more different from those obtained with the Munsell chips. They did not show a peak around unique yellow (Supplementary Figure S14c). Their correlation with the singularities of the Munsell chips explained only 40% of the variance ($r = 0.63$, $p < 0.001$), which is marginally significantly below the 50% criterion ($z = -1.7$, $p = 0.09$). The correlation with focal colors explained only 14% of the variance ($r = 0.38$, $p < 0.001$), which is significantly below 41% ($z = -4.5$, $p < 0.001$) but not significantly below the 20.4% defined by the 50% criterion ($p = 0.27$).

Using different kinds of reflectances affected the pattern of singularities and reduced their relationship to focal colors and unique hues. However, the singularity indices are still clearly related to focal colors and unique hues for all maximally saturated reflectances. Hence, the effect of using different reflectances was not strong enough to completely undermine the

relationship between singularities, focal colors, and unique hues.

Uniformly saturated reflectances

For the uniformly saturated reflectances, the peaks of singularities do not coincide with unique hues (black circles in Figure 14b, d, and f and Supplementary Figure S14b, d). The light bars in Figure 15 show the variance explained with singularities for uniformly saturated reflectances. These bars were much lower than the dark ones for maximally saturated reflectances, showing the impact of Munsell chroma on the pattern of singularity indices.

The singularities of the uniformly saturated Munsell chips ("MC-uni") explained only 34% of the variance with the singularities of the maximally saturated Munsell chips ($r = 0.58$, $p < 0.001$) and only 2% with focal color choices ($r = 0.15$, $p < 0.01$). Although these correlations were still significantly positive, they were both significantly reduced below the criterion of 50% ($z = -2.8$, $p < 0.01$) and 20.4% ($z = -4.2$, $p < 0.001$), respectively.

The singularity indices of the uniformly saturated RGB reflectances ("RGB-uni" and "RGB-uni D65") shared only 39% and 37% of the variance with those of maximally saturated Munsell chips, respectively ($r = 0.62$ and 0.61, both $p < 0.001$). These were marginally significantly ($z = -1.9$, $p = 0.06$) and significantly below 50% ($z = -2.3$, $p < 0.05$). Accordingly, the correlations with focal colors were also below the criterion of 20.4% ($z = -3.2$, $p < 0.01$ and $z = -3.4$, $p < 0.001$), explaining only 5% of the variance. However, again these correlations with focal colors were still significant ($r = 0.23$ and 0.21, both $p < 0.001$).

In contrast, the pattern of singularities for the fundamental metamers of the uniformly saturated Munsell chips under illuminant E (Figure 14f) and D65 (Supplementary Figure S14d) had barely anything in common with that of the maximally saturated Munsell chips. As a result, in Figure 15 the bars for uniformly saturated reflectances based on fundamental metamers ("FC-uni" and "FC-uni D65") were close to zero. The singularities for those reflectances shared only 1% ($r = 0.10$, $p = 0.07$) and 2% ($r = 0.15$, $p = 0.01$) of variance with the singularities for the maximally saturated Munsell chips, respectively. While these correlations were still marginally significantly and significantly different from zero, they were significantly lower than 50% ($z = -9.8$ and -9.2, both $p < 0.001$). These differences were so strong that there were no significant correlations with focal colors ($r = -0.10$, $p = 0.06$ and $r = -0.05$, $p = 0.35$), which implies that they were also lower than 20.4% as defined by the 50% criterion (both $p < 0.001$).

These results show that the effect of Munsell chroma and the effect of using different kinds of reflectances completely annihilate the relationship between singularities and focal colors.

Munsell chroma versus type of reflectance

The following analyses aimed to disentangle the effects of Munsell chroma, type of reflectance, and the illuminant used to create metameric reflectances. Comparing the left (panels a, c, and e) and right (panels b, d, and f) columns of Figure 14 and Supplementary Figure S14 allows for the appreciation of the impact of differences in Munsell chroma on the pattern of singularities. The patterns of singularities for the uniformly saturated reflectances in the right column of Figure 14 and Supplementary Figure S14 differ from those for the maximally saturated reflectances in the respective left columns. To quantify the similarities between these patterns, we calculated correlations between the singularity indices on the left and right sides for each row in Figure 14 and Supplementary Figure S14. Supplementary Table S9 provides details. All correlations were significant, showing systematic similarities between the singularities of maximally and uniformly saturated variants of each kind of reflectance (i.e., each row in Figure 14 and Supplementary Figure S14). Nevertheless, they explained less than 50% of variance, which indicates a strong effect of Munsell chroma on the pattern of singularities.

Comparing the rows within each column of Figure 14 and Supplementary Figure S14 allows for assessing whether the spectral characteristics of the reflectances play a role in the pattern of singularities even when the LMS signal produced by these reflectances is the same under white light. Above, the singularities of the uniformly saturated reflectances were compared with those of the maximally saturated Munsell chips in Figure 14a. Here, we compared them to the singularities of the uniformly saturated Munsell chips in Figure 14b to get an idea of how strongly the different types of reflectances affect singularities independently of the effect of Munsell chroma. For this purpose, we calculated the correlations between singularity indices for the uniformly saturated Munsell chips in Figure 14b and those for the uniformly saturated artificial reflectances in the right columns of Figure 14 (panels d and f) and Supplementary Figure S14 (panels b and d). Supplementary Table S10 provides detailed results.

Singularities for uniformly saturated RGB reflectances (Figure 14d and Supplementary Figure S14b) were very similar to those for uniformly saturated Munsell chips. The correlations explained 84% ($r = 0.92$, $p < 0.001$) and 81% ($r = 0.90$, $p < 0.001$) of the variance. Singularity indices of the reflectances based on fundamental metamers (Figure 14e and Supplementary Figure S14d) were more different from the ones for the uniformly saturated Munsell chips. The singularity indices of the fundamental metamers under illuminant E shared only 21% ($r = 0.46$, $p < 0.001$) of the variance with those for the uniformly saturated Munsell chips, and those under illuminant D65 shared only 16% ($r = 0.41$, $p < 0.001$). These latter results indicate a strong impact of the type of reflectance on the pattern of singularities when reflectances are uniformly saturated.

Finally, the comparison between the artificial reflectances in Figure 14c through f and Supplementary Figure S14 allows for the appreciation of the impact of assuming illuminant E or D65 for the metamers. The artificial reflectances produced with illuminant E and illuminant D65 yielded very similar results. As shown in Supplementary Table S11, the singularity indices of the corresponding reflectances produced under illuminants E and D65 were highly correlated (minimum $r = 0.81$). These results indicate that the difference between reflectances that were metameric under illuminants E and D65 was of minor importance for the pattern of singularities.

Taken together, these results highlight the importance of Munsell chroma for the pattern of singularities. At the same time, the results for the reflectances based on fundamental metamers suggest that the pattern of singularities also varies across surfaces that are metameric under white light (illuminant E and illuminant D65). As a result, both Munsell chroma and the type of reflectances affect the relationship of singularities to focal colors and unique hues, as observed in the section above. Combining both effects completely destroyed this relationship.

Interaction with illuminants and sensors

We also inspected whether combining different illuminants and sensors with the reflectances results in interaction effects. Supplementary Figure S15 provides the explained variances in the format of Figure 15 for these additional analyses.

First, we examined singularity patterns across reflectances under random-spline illuminants instead of natural illuminants. Although there were some slight differences in the amount of explained variance for each type of reflectance (cf. Supplementary Figure S15a, c), overall the results were mainly the same as with natural illuminants: There was a consistent effect of Munsell chroma across all reflectances and smaller modulations due to the different types of reflectances.

In contrast, varying sensors together with reflectances had a much stronger effect on the pattern of singularities. In particular, changing the sensors had much stronger effects on singularities when combined with reflectances other than the maximally saturated

Munsell chips. This becomes particularly clear when looking at the results across reflectances for orthogonal sensors (cf. Figure 9c). Supplementary Figure S15b and d illustrates the explained variances. As reported above, these sensors produced a highly similar pattern of singularities for maximally saturated Munsell chips. However, the singularity pattern strongly changed compared with that obtained with human cones for all other reflectances, including maximally saturated artificial reflectances and uniformly saturated Munsell chips (Supplementary Figure S15b). As a consequence, singularity patterns were only very weakly or not at all correlated with focality for orthogonal sensors combined with those kinds of reflectances (Supplementary Figure S15d). These results indicate that, in general, singularities depend on the interaction of sensors and reflectances. However, reflectances of maximally saturated Munsell chips have properties that produce patterns of singularities that are stable across illuminants and sensors.

Discussion

The comparison between maximally and uniformly saturated reflectances showed that the singularity index and its relationship to focal colors and unique hues strongly depend on variations of Munsell chroma. The results with artificial reflectances indicated that differences in the spectral characteristics of reflectances that look the same under white light also play a role in singularities and their relationship to focal colors and unique hues.

Munsell chroma

The importance of Munsell chroma for the relationship between singularities and focal colors seems very clear since the relationship was much lower for uniformly saturated reflectances than for maximally saturated reflectances. The question arises of why Munsell chroma strongly modulates this relationship. We discuss this question in three steps.

First, we wonder where the pattern of singularities for uniformly saturated reflectances comes from. For maximally saturated Munsell chips, the relationship between singularities and chroma is clear from Figure 5b. In contrast, uniformly saturated reflectances were more uniform and lower in Munsell chroma than the maximally saturated reflectances. If singularities depend on Munsell chroma, singularity indices for uniformly saturated Munsell chips should be lower and more uniform than those for maximally saturated reflectances. Figure 14 and Supplementary Figure S14 do not allow for comparing the sizes of singularities between maximally and uniformly saturated reflec-
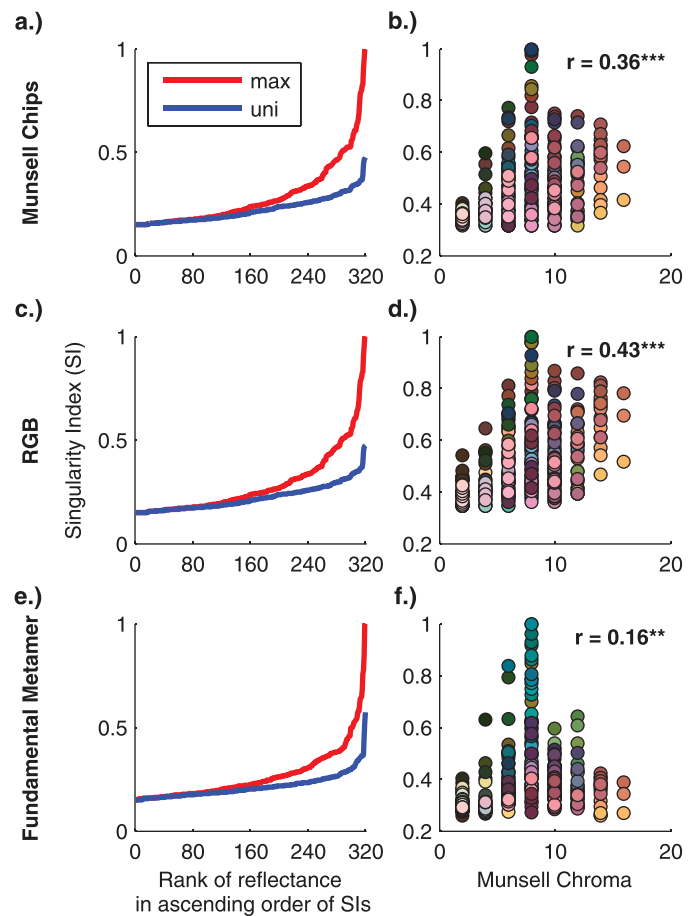

Figure 16. The variation of singularity indices for uniformly saturated Munsell chips. The left side of the figure (panels a, c, and e) shows the size of singularity indices for maximally and uniformly saturated Munsell chips, reflectances based on RGBs, and fundamental metamers (under illuminant E), respectively. For these graphics, singularity indices were normalized for maximally and uniformly saturated reflectances together in order to compare the size across both kinds of reflectances. The red and blue curves show the singularity indices for the maximally and uniformly saturated reflectances, respectively, sorted in ascending order of the singularity indices. The *x*-axis corresponds to the rank of the reflectance within that order, and the *y*-axis corresponds to the singularity index of that reflectance. The right side (panels b, d, and f) shows the correlation between singularity indices and Munsell chroma for the uniformly saturated reflectances. The format is the same as that in Figure 5b. Note that the maximally saturated reflectances reach much higher singularities and hence cover a much larger range of singularities compared with the uniformly saturated ones (left side). Moreover, even for uniformly saturated Munsell chips, singularities are slightly related to Munsell chroma (right side).

tances because the contours in each panel of those figures range from the minimum to the maximum singularity within the respective data set. The left side of Figure 16 (panels a, c, and e) provides such a

comparison between maximally (red curve) and uniformly (blue curve) saturated reflectances. The singularity indices for uniformly saturated reflectances do not reach as high as those for maximally saturated reflectances, and as a result the range over which singularities vary is much smaller than for maximally saturated reflectances. This implies that the contours shown on the right side of Figure 14 correspond to a smaller range of variation than those shown on the left side. Hence the pattern of singularities is much less pronounced for uniformly saturated Munsell chips than for maximally saturated Munsell chips.

At the same time, even our set with uniform Munsell chroma did not result in the same Munsell chroma for all Munsell chips because Munsell chips at high and low lightness only reach very low Munsell chroma. The right side of Figure 16 (panels b, d, and f) illustrates the correlation between Munsell chroma and singularity indices for the uniformly saturated reflectances in the same format as Figure 5b for the maximally saturated Munsell chips. Despite the reduced variation in Munsell chroma, there are still correlations between singularities and Munsell chroma. Hence, some variation of the singularity indices for uniformly saturated Munsell chips may be due to variation in Munsell chroma. This may also partly explain why there are still some similarities between maximally and uniformly saturated reflectances, as observed above (cf. Supplementary Table S9).

Taken together, these additional results further highlight the role of Munsell chroma in sensory singularities.

Second, the focal color distributions used in our study were measured with maximally saturated Munsell chips. The question arises of whether these measurements of focal colors are appropriate for examining the relationship with singularities for uniformly saturated reflectances.

Observers tend to choose more saturated colors as prototypes of chromatic categories. The reflectances in the uniformly saturated sets are almost never chosen as typical colors because their Munsell chroma is too low for chromatic and too high for achromatic color categories (e.g., figure 8 in Olkkonen et al., 2010). Moreover, color categories change depending on Munsell chroma. For example, the *red* category is not defined at low chroma. In contrast, *brown* and *gray* categories become larger with decreasing saturation (e.g., figure 8 in Olkkonen et al., 2010). Consequently, the distribution of focality across Munsell hue and value may be different from the one of maximally saturated Munsell chips.

For these reasons, the lack of a relationship between singularities for uniformly saturated reflectances and the focal colors obtained with maximally saturated Munsell chips might support rather than contradict the relationship between singularities and focal colors. The fact that singularities are lower and more uniform and show a different pattern for uniform Munsell chroma might just reflect the fact that these reflectances would also result in lower levels and different distributions of focality. It is possible that the distribution of focal colors would be more similar to the distribution of singularity indices for uniformly saturated reflectances if focal colors were measured with a set of uniformly colored reflectances. It is difficult to test this idea. Because observers do not choose desaturated colors as prototypes, a distribution of focality across hue and lightness may not be directly measured with colors as desaturated as our uniformly saturated sets.

In contrast to focal colors, unique hues are solely defined by hue, not saturation. Munsell hues that were identified as pure red, yellow, green, and blue with maximally saturated Munsell chips should be similar for desaturated Munsell chips. The fact that the highest singularities of uniformly saturated reflectances were not close to these hues implies that there is really no relationship between singularities and unique hues for uniformly saturated reflectances.

We further explored the origin of the relationship between singularities and focal colors for maximally saturated Munsell chips. The consistency of color naming is a way to measure the strength of category membership across colors (e.g., Olkkonen et al., 2010; Olkkonen, Hansen, & Gegenfurtner, 2009). Figure 17 illustrates the relationship of focal colors and singularities to category consistency for maximally saturated Munsell chips as measured for German observers by Olkkonen et al. (2010). Category consistency is not correlated to focal color choices in the World Color Survey ($r = 0.06$, $p = 0.25$; in a partial correlation controlling for Munsell chroma: $r = -0.08$, $p = 0.13$). Moreover, categorical consistency is only marginally significantly correlated to the singularity index ($r = 0.11$, $p = 0.06$; see also Olkkonen et al., 2009), and this correlation is even negative when controlling for Munsell chroma in a partial correlation ($r = -0.19$, $p < 0.001$). The negative correlation might be due to the fact that there are additional categories between red, yellow, green, and blue, such as orange or purple. These categories have peak consistencies where singularities are low.

In any case, these results show that neither focal colors nor singularities are directly related to category membership. As a consequence, it remains unclear what exactly constitutes the relationship between focal colors and singularities for maximally saturated colors apart from Munsell chroma.

Third, the question arises of how Munsell chroma may modulate the relationship between singularities on the one hand and focal and unique hues on the other. What are the characteristics of Munsell chroma that
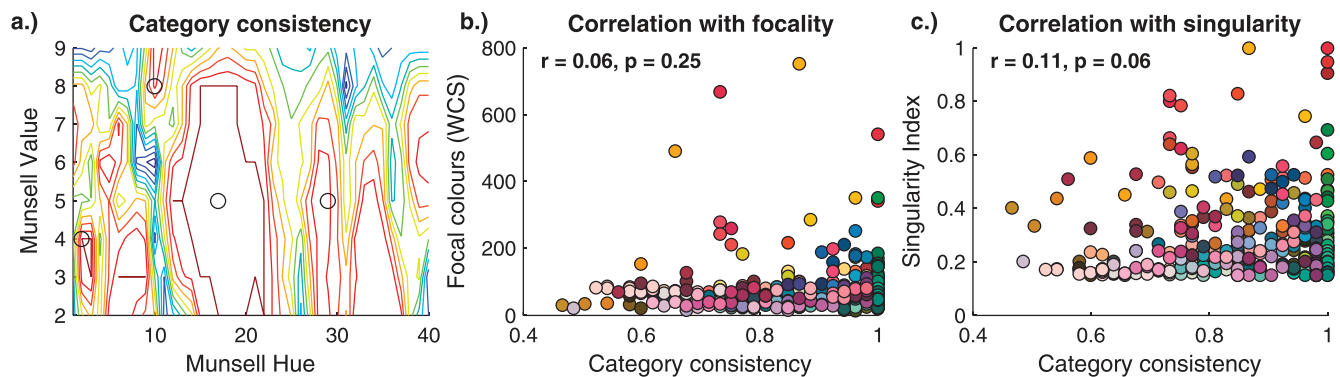
Figure 17. Category consistency. Panel a shows the categorical consistency across Munsell hue and value for maximally saturated Munsell chips. Contours refer to categorical consistency of German observers as measured by Olkkonen et al. (2010) across different illuminations. The format is the same as that in Figure 4. Panel b illustrates the relationship between category consistency and focal color choices measured in the World Color Survey (cf. Figure 4b). The *x*-axis corresponds to category consistency in relative frequencies of same categorizations, and the *y*-axis corresponds to focal color choices. Panel c shows the relationship between category consistency and singularities. The *x*-axis corresponds to category consistency, and the *y*-axis corresponds to the singularity index. Apart from that, the format in panels b and c is the same as that in Figure 5. Note that category consistency is correlated neither with focality nor with singularity.

affect both singularities and focal colors and unique hues?

Munsell chroma is supposed to reflect perceived chroma. However, it is only an approximate control for perceived chroma across hues. As a result, even if Munsell chroma were the same across hues, this would not mean that the actual perceived chroma would be perfectly equal across hues. Most importantly, perceived chroma does not have maxima around focal colors, neither when measured in terms of discriminable differences from gray (Witzel et al., in prep) nor when measured in terms of subjective appearance (Witzel & Franklin, 2014). Hence, the relationship between focal colors and maximally saturated Munsell chroma is a particularity of the Munsell system that does not exist between focal colors and perceived chroma.

It is possible that observers across different languages tend to choose colors with higher chroma as prototypes of chromatic color categories. In this case, it is even possible that the cross-cultural regularities in prototype choices are due to the differences in perceived chroma across the maximally saturated Munsell chips (Witzel & Franklin, 2014).

At the same time, a possible explanation for the relationship between singularities and maximally saturated Munsell chips might be that those Munsell chips reach particular levels of *excitation purity*, which is the radial difference in chromaticity from the white point. For a given hue, Munsell chroma is also related to excitation purity. The higher the Munsell chroma for a given hue, the farther away the chromaticity coordinates are from the white point. When calculating singularity indices for all Munsell chips, singularity indices increase with purity (cf. figure 4 of Philipona & O'Regan, 2006). If both the measurement of focal

colors and the distribution of singularities are artifacts of the distribution of Munsell chroma, the relationship between singularities and focal colors could be explained by the stimulus sampling of Munsell chips.

However, in additional analyses Philipona and O'Regan (2006) showed that at comparable levels of purity, singularities had local maxima around unique hues. This was the case across different levels of Munsell chroma ("crests" in figure 4 of Philipona & O'Regan, 2006). Hence, the relationship between singularities and unique hues seems to hold for equal levels of colorimetric purity but not for equal levels of Munsell chroma.

The perceived chroma across hues is still more variable for equal levels of excitation purity than for equal Munsell chroma. Excitation purity is related to how close a light spectrum is to monochromatic light. The fact that the relationship between singularities and unique hues is much more stable across equal levels of purity than across equal levels of Munsell chroma suggests that the relationship between singularities and unique hues might be due to spectral characteristics rather than to perceived chroma.

Metameric spectra

Different types of reflectances had a different impact on the pattern of singularities and their relationship to focal colors and unique hues. First of all, the high similarity between the singularities for the two kinds of metameric matches (under illuminants E and D65) is not surprising because illuminants E and D65 are very similar and reflect light in similar ways (cf. Figure 13c through f and Supplementary Figure S13). Consequently, the reflected LMS signals of these surfaces are

very similar under these illuminants, which explains the similarity of the singularity indices. Taken together, the findings with these two kinds of metameric matches indicate that the gist of our results does not depend on the white illuminant we assume for the metameric matches.

Despite their different reflectance spectra, RGB-based reflectances produced similar results compared with the original Munsell chips. The main difference between the RGB-based spectra and those of the Munsell chips is in the two enormous peaks at long wavelengths in the RGB spectra (cf. Figure 13c, d). These peaks result from the narrow-band spectrum of the red primary. It seems that these peaks barely affect the pattern of singularities and their relationship to focal colors and unique hues. At the same time, the red and green primaries roughly coincide with unique and focal red and green. The blue primary is also close to unique and focal blue, being just slightly more reddish (e.g., Witzel et al., in prep). The mixture of the maximum red and green primaries produces a color that is close to focal yellow. As a result, RGB primaries may produce particularly saturated colors around focal red, yellow, green, and blue. The high saturation around the colors may explain why the maximally saturated RGB reflectances produced almost as high correlations between singularities and focal colors as the maximally saturated Munsell chips.

At the same time, the results with fundamental metamers indicated that not all surfaces that look like the typical or unique red, yellow, green, or blue yield particularly high singularity indices. In particular, there exist metameric reflectances that produce the same LMS signal as the Munsell chips under white light (illuminant E or illuminant D65) but result in different patterns of singularities.

Some of the artificial reflectances took values that cannot occur in physical reflectances of real surfaces (Figure 13c through f). However, our main findings do not depend on whether the reflectances are physically realizable. Most importantly, the strong similarity of the singularity patterns between the different kinds of maximally saturated reflectances occurred despite the values of some artificial reflectances being outside the interval between 0 and 1 (cf. Figure 14a, c, and e).

Moreover, additional analyses showed that the changes in the singularity patterns that occurred when using more uniform Munsel chroma and when using different kinds of reflectances also occurred when all reflectances were in the interval between 0 and 1. In addition to the artificial reflectances based on RGBs and fundamental metamers, we produced artificial reflectances based on nonoverlapping Gaussian, linear, and step functions, such as those used for the artificial sensors in Figure 9c, e, and j. Details on these additional analyses are provided in the Additional

kinds of reflectances section of the supplementary materials (Supplementary Figures S16 and S17 and Supplementary Table S12). In particular, when using linear and step functions, all uniformly saturated reflectances were physically realizable (i.e., within the interval [0, 1]; cf. Supplementary Figure S16d, f). Nevertheless, these reflectances still produced strongly different singularities compared with the maximally saturated Munsell chips ($R^2 = 22\%$ and 36%) and were barely correlated with focal colors ($R^2 = 1\%$ and 4%; cf. Supplementary Table S12). These results confirm the strong effect of Munsell chroma even when all reflectances are physically realizable. Furthermore, these artificial reflectances also produced slightly different singularity patterns compared with the uniformly saturated Munsell chips, hence confirming an effect of the type of reflectance on singularities. As a consequence, the findings with artificial reflectances based on RGBs and fundamental metamers are representative for physically realizable reflectances.

The difficulty of producing physically realizable reflectances that are metameric with the light reflected by maximally saturated Munsell chips under white illuminations indicates that the unequal distribution of maximal Munsell chroma across hue and lightness is bound to the reflectance spectra of Munsell chips. Using a different set of pigments to produce color chips would result in different reflectance spectra, which would allow for a different distribution of maximal chroma across hue and lightness. Given the dependence of singularities on the distribution of maximal Munsell chroma, maximally saturated color chips based on pigments other than those of Munsell chips might also produce a different pattern of singularities, which might not be related to focal colors and unique hues.

Finally, we also observed that the stability of the pattern of singularities across different kinds of sensors is a particularity of the maximally saturated Munsell chips. The pattern of singularities for maximally saturated reflectances other than Munsell chips, and for all uniformly saturated reflectances, is affected much more strongly by changes in the sensitivities of the sensors (cf. the Interaction with illuminants and sensors section).

Taken together, our findings suggest that there is something particular about the reflectances of Munsell chips that produces the strong relationship between singularities, focal colors, and unique hues. For example, it might be that pigments are particularly pure for the Munsell chips that correspond to focal colors and unique hues. In this case, these chips would have reflectances with narrower bandwidth and, hence, higher colorimetric purity. These peaks in colorimetric purity might be the origin of the observations that those chips have the highest available chroma in the

Munsell system and that they have the highest singularities.

This idea is further supported by the results of nonnegative matrix factorization. The principal components have partly negative spectral power, and hence the principal components themselves may not physically exist (e.g., as reflectances of pigments; cf. Supplementary Figure S12). In contrast, nonnegative matrix factorization provides nonnegative linear basis functions that may exist as real reflectances of pigments. Munsell reflectances can be approximated using four nonnegative basis functions that strongly correspond to red, yellow, green, and blue (Buchsbaum & Bloch, 2002). Hence, the reason why Munsell chips exist at particularly high Munsell chroma for these hues might be that these hues correspond to pure component spectra.

Conclusions

The present study investigated whether characteristics of illuminants, reflectances, or sensors are the main determinants of the relationship between focal colors, unique hues, and the singularities in the variation of LMS signals across changes in illumination. We found that the relationship between singularities, focal colors, and unique hues is stable across a wide range of illuminations and across fundamentally different sensors as long as the illuminants and the sensitivities of these sensors extend to both ends of the visible spectrum. In contrast, the characteristics of the reflectances strongly affected the distribution of singularities across colors and were crucial for the relationship between singularities, focal colors, and unique hues. Moreover, it turned out that something particular about the reflectances of maximally saturated Munsell chips establishes a robust relationship between singularities, focal colors, and unique hues. In fact, when reflectances other than maximally saturated Munsell chips are used, singularities are affected by the type of sensors. The finding that reflectances and Munsell chroma play a crucial role in the relationship between singularities, focal colors, and unique hues points to three major paths for future research on sensory singularities.

First, the original motivation for investigating sensory singularities was to show that color language and color appearance would be related to objects with which human observers interact under changing illuminations in their natural visual environment. However, Munsel chips and the other reflectances investigated here are not representative samples of natural reflectances. Hence, the question arises of how the findings about the relationship between singulari-

ties, focal colors, and unique hues apply to reflectances in the natural environment. There is evidence for a positive answer to this question. Natural reflectances fall into a limited set of mainly three classes (Osorio & Bossomaier, 1992) and may be represented using three principal components (Chiao et al., 2000). Moreover, the principal components of Munsell chips may be used to reconstruct natural reflectances with high precision (Jaaskelainen, Parkkinen, & Toyooka, 1990), indicating a similarity between the reflectances of Munsell chips and natural surfaces. Finally, some of the results of Philipona and O'Regan (2006) supported the idea that singularities have similar peaks for natural reflectances as for Munsell chips. In an ongoing follow-up study we provide further evidence for this idea (Witzel & O'Regan, 2014).

Second, the question arises of which are the precise characteristics of the reflectance spectra that modulate sensory singularities. Answers to this question would allow for clarifying how reflectance properties modulate the relationship between sensory singularities, color language, and color appearance. A possible analytical approach for determining the characteristics of singular reflectances could consist of exploring metameric black space. Previous studies have used this approach to determine the space of illuminants under which all surfaces reflect an LMS signal along a line, implying that this LMS signal is singular (Brainard, Wandell, & Cowan, 1989; Burns et al., 1989). The role of illuminants and reflectances in this approach might be reversed in order to determine the space of reflectances that are singular under all natural illuminants.

Finally, it is an open question how sensory singularities are translated into perception. In particular, it is not clear how sensory singularities relate to adaptation and color constancy. Moreover, Munsell chroma is not an accurate perceptual attribute and might produce spurious effects on the pattern of singularities. Hence, better ways to control perceptual attributes must be found to relate samples of surface colors and sensory singularities to color perception. For this reason, future research needs to investigate how sensory singularities are related to perceived attributes of color, such as perceived chroma, hue, and lightness; perceived color variegation; and color constancy.

Keywords: color appearance, color categories, color constancy, color vision, unique hues

Acknowledgments

References

Abramov, I., & Gordon, J. (1994). Color appearance: On seeing red—Or yellow, or green, or blue. *Annual Review of Psychology, 45,* 451–485, doi:10.1146/annurev.ps.45.020194.002315.

Bachy, R., Dias, J., Alleysson, D., & Bonnardel, V. (2012). Hue discrimination, unique hues and naming. *Journal of the Optical Society of America A, 29*(2), A60–A68, doi:10.1364/JOSAA.29.000A60.

Brainard, D. H., Wandell, B. A., & Cowan, W. B. (1989). Black light: How sensors filter spectral variation of the illuminant. *IEEE Transactions on Biomedical Engineering, 36*(1), 140–149, doi:10.1109/10.16459.

Brown, A. M., Lindsey, D. T., & Guckes, K. M. (2011). Color names, color categories, and color-cued visual search: Sometimes, color perception is not categorical. *Journal of Vision, 11*(12):2, doi:10.1167/11.12.2. [PubMed] [Article]

Brown, R. W., & Lenneberg, E. H. (1954). A study in language and cognition. *Journal of Abnormal and Social Psychology, 49*(3), 454–462.

Buchsbaum, G., & Bloch, O. (2002). Color categories revealed by non-negative matrix factorization of Munsell color spectra. *Vision Research, 42*(5), 559–563.

Burns, S. A., Cohen, J. B., & Kuznetsov, E. N. (1989). Multiple metamers: Preserving color matches under diverse illuminants. *Color Research & Application, 14*(1), 16–22, doi:10.1002/col.5080140106.

Chiao, C. C., Cronin, T. W., & Osorio, D. (2000). Color signals in natural scenes: Characteristics of reflectance spectra and effects of natural illuminants. *Journal of the Optical Society of America A, 17*(2), 218–224.

Cohen, J. B. (1964). Dependency of the spectral reflectance curves of the Munsell-color chips. *Psychonomic Science, 1*(12), 369–370.

Cohen, J. B., & Kappauf, W. E. (1982). Metameric color stimuli, fundamental metamers, and Wys-zecki's metameric blacks. *American Journal of Psychology, 95*(4), 537–564.

Collier, G. A. (1973). Review of "Basic Color Terms: Their Universality and Evolution." *Language, 49*(1), 245–248.

Cropper, S. J., Kvansakul, J. G., & Little, D. R. (2013). The categorisation of non-categorical colours: A novel paradigm in colour perception. *PLoS One, 8*(3), e59945, doi:10.1371/journal.pone.0059945.

Das, S. R., & Sastri, V. D. P. (1965). Spectral distribution and color of tropical daylight. *Journal of the Optical Society of America, 55*(3), 319–322, doi:10.1364/JOSA.55.000319.

Dixon, E. R. (1978). Spectral distribution of Australian daylight. *Journal of the Optical Society of America, 68*(4), 437–450, doi:10.1364/Josa.68.000437.

Fisher, R. A. (1921). On the "probable error" of a coefficient of correlation deduced from a small sample. *Metron, 1,* 3–32.

Gegenfurtner, K. R. (2003). Cortical mechanisms of colour vision. *Nature Reviews Neuroscience, 4,* 563–572.

Gegenfurtner, K. R., & Kiper, D. C. (2003). Color vision. *Annual Review of Neuroscience, 26*(1), 181–206.

Jaaskelainen, T., Parkkinen, J., & Toyooka, S. (1990). Vector-subspace model for color representation. *Journal of the Optical Society of America A, 7*(4), 725–730, doi:10.1364/JOSAA.7.000725.

Judd, D. B., Macadam, D. L., Wyszecki, G., Budde, H. W., Condit, H. R., Henderson, S. T., & Simonds, J. L. (1964). Spectral distribution of typical daylight as a function of correlated color temperature. *Journal of the Optical Society of America, 54*(8), 1031–1036.

Kay, P., & Regier, T. (2003). Resolving the question of color naming universals. *Proceedings of the National Academy of Sciences, USA, 100*(15), 9085–9089.

Koenderink, J. J. (2010). The prior statistics of object colors. *Journal of the Optical Society of America A, 27*(2), 206–217.

Kohonen, O., Parkkinen, J., & Jaaskelainen, T. (2006). Databases for spectral color science. *Color Research and Application, 31*(5), 381–390, doi:10.1002/Col.20244.

Kuehni, R. G., Shamey, R., Mathews, M., & Keene, B. (2010). Perceptual prominence of Hering's chromatic primaries. *Journal of the Optical Society of America A, 27*(2), 159–165.

Lindsey, D. T., & Brown, A. M. (2006). Universality of

color names. *Proceedings of the National Academy of Sciences, USA, 103*(44), 16608–16613.

Lindsey, D. T., & Brown, A. M. (2009). World Color Survey color naming reveals universal motifs and their within-language diversity. *Proceedings of the National Academy of Sciences, USA, 106*(47), 19785–19790, doi:10.1073/pnas.0910981106.

Lindsey, D. T., Brown, A. M., Reijnen, E., Rich, A. N., Kuzmova, Y. I., & Wolfe, J. M. (2010). Color channels, not color appearance or color categories, guide visual search for desaturated color targets. *Psychological Science, 21*(9), 1208–1214, doi:10. 1177/0956797610379861.

Logvinenko, A. D., Funt, B., & Godau, C. (2014). Metamer mismatching. *IEEE Transactions on Image Processing, 23*(1), 34–43, doi:10.1109/TIP. 2013.2283148.

Malkoc, G., Kay, P., & Webster, M. A. (2005). Variations in normal color vision. IV. Binary hues and hue scaling. *Journal of the Optical Society of America A, 22*(10), 2154–2168.

Maloney, L. T. (1986). Evaluation of linear models of surface spectral reflectance with small numbers of parameters. *Journal of the Optical Society of America A, 3*(10), 1673–1683.

Maloney, L. T. (1999). Physics-based approaches to modeling surface color perception. In K. R. Gegenfurtner & L. T. Sharpe (Eds.), *Color vision: From genes to perception* (pp. 387–416). Cambridge, United Kingdom: Cambridge University Press.

Mollon, J. D. (2009). A neural basis for unique hues? *Current Biology, 19*(11), R441–R442, R442–R443, doi:10.1016/j.cub.2009.05.008.

Munsell, A. H. (1912). A pigment color system and notation. *American Journal of Psychology, 23*(2), 236–244, doi:10.2307/1412843.

Munsell Color Services. (2007). *The Munsell book of color: Glossy collection*. Grandville, MI: X-Rite.

O'Regan, J. K. (2011). *Why red doesn't sound like a bell: Understanding the feel of consciousness*. New York, NY: Oxford University Press.

O'Regan, J. K., & Noe, A. (2001a). A sensorimotor account of vision and visual consciousness. *Behavioural and Brain Sciences, 24*(5), 939–973, 973–1031.

O'Regan, J. K., & Noe, A. (2001b). What it is like to see: A sensorimotor theory of visual experience. *Synthese, 129,* 79–103.

Olkkonen, M., Hansen, T., & Gegenfurtner, K. R. (2009). Categorical color constancy for simulated surfaces. *Journal of Vision, 9*(12):6, 1–18, doi:10. 1167/9.12.6. [PubMed] [Article]

Olkkonen, M., Witzel, C., Hansen, T., & Gegenfurtner, K. R. (2010). Categorical color constancy for real surfaces. *Journal of Vision, 10*(9):16, 1–22, doi:10. 1167/10.9.16. [PubMed] [Article]

Osorio, D., & Bossomaier, T. R. J. (1992). Human cone-pigment spectral sensitivities and the reflectances of natural surfaces. *Biological Cybernetics, 67*(3), 217–222.

Parkkinen, J. P. S., Hallikainen, J., & Jaaskelainen, T. (1989). Characteristic spectra of Munsell colors. *Journal of the Optical Society of America A, 6*(2), 318–322, doi:10.1364/Josaa.6.000318.

Philipona, D. L., & O'Regan, J. K. (2006). Color naming, unique hues, and hue cancellation predicted from singularities in reflection properties. *Visual Neuroscience, 23*(3–4), 331–339, doi:10.1017/ S0952523806233182.

Regier, T., Kay, P., & Cook, R. S. (2005). Focal colors are universal after all. *Proceedings of the National Academy of Sciences, USA, 102*(23), 8386–8391, doi:10.1073/pnas.0503281102.

Regier, T., Kay, P., & Khetarpal, N. (2007). Color naming reflects optimal partitions of color space. *Proceedings of the National Academy of Sciences, USA, 104*(4), 1436–1441, doi:10.1073/pnas. 0610341104.

Romero, J., Garcia-Beltran, A., & Hernandez-Andres, J. (1997). Linear bases for representation of natural and artificial illuminants. *Journal of the Optical Society of America A, 14*(5), 1007–1014, doi:10. 1364/Josaa.14.001007.

Romney, A. K., & Indow, T. (2003). Munsell reflectance spectra represented in three-dimensional Euclidean space. *Color Research and Application, 28*(3), 182–196, doi:10.1002/Col.10144.

Rosch Heider E. (1972). Universals in color naming and memory. *Journal of Experimental Psychology, 93*(1), 10–20.

Sastri, V. D. P., & Das, S. R. (1966). Spectral distribution and color of north sky at Delhi. *Journal of the Optical Society of America, 56*(6), 829–830, doi:10.1364/Josa.56.000829.

Sastri, V. D. P., & Das, S. R. (1968). Typical spectral distributions and color for tropical daylight. *Journal of the Optical Society of America, 58*(3), 391–398, doi:10.1364/Josa.58.000391.

Smith, V. C., & Pokorny, J. (1975). Spectral sensitivity of the foveal cone photopigments between 400 and 500 nm. *Vision Research, 15*(2), 161–171.

Stiles, W. S., & Burch, J. M. (1959). NPL colour-matching investigation: Final report. *Optica Acta, 6*(1), 1–26.

Stockman, A., & Sharpe, L. T. (2000). The spectral

sensitivities of the middle- and long-wavelength-sensitive cones derived from measurements in observers of known genotype. *Vision Research, 40*(13), 1711–1737.

Valberg, A. (2001). Unique hues: An old problem for a new generation. *Vision Research, 41*(13), 1645–1657.

Vazquez-Corral, J., O'Regan, J. K., Vanrell, M., & Finlayson, G. D. (2012). A new spectrally sharpened sensor basis to predict color naming, unique hues, and hue cancellation. *Journal of Vision, 12*(6): 7, 1–14, doi:10.1167/12.6.7. [PubMed] [Article]

Webster, M. A., Webster, S. M., Bharadwaj, S., Verma, R., Jaikumar, J., Madan, G., & Vaithilingham, E. (2002). Variations in normal color vision. III. Unique hues in Indian and United States observers. *Journal of the Optical Society of America A, 19*(10), 1951–1962.

Witzel, C. (2011). Unterschiede in der Farbwahrnehmung [Translation: Differences in color perception]. In A. Groh (Ed.), *Was ist Farbe? Bunte Beiträge aus der Wissenschaft* [Translation: *What is color? Diverse contributions from science*] (pp. 39–62). Berlin, Germany: Weidler.

Witzel, C., Cinotti, F., & O'Regan, J. K. (2014). *How color language is shaped by the variability of reflected light under changes of illumination.* Paper presented at the AISB convention 2014 of the Society for the study of Artificial Intelligence and Simulation of Behaviour, Goldsmiths, University of London, London, UK. Retrieved from doc.gold.ac.uk/aisb50/AISB50-S20/aisb50-S20-witzel-paper.pdf

Witzel, C., & Franklin, A. (2014). Do focal colors look particularly "colorful"? *Journal of the Optical Society of America A, 31*(4), A365–A374, doi:10.1364/JOSAA.31.00A365.

Witzel, C., & Gegenfurtner, K. R. (2011). Is there a lateralized category effect for color? *Journal of Vision, 11*(12):16, 1–25, doi:10.1167/11.12.16. [PubMed] [Article]

Witzel, C., & Gegenfurtner, K. R. (2013). Categorical sensitivity to color differences. *Journal of Vision, 13*(7):1, 1–33, doi:10.1167/13.7.1. [PubMed] [Article]

Witzel, C., & Gegenfurtner, K. R. (2014). Category effects on colour discrimination. In W. Anderson, C. P. Biggam, C. A. Hough, & C. J. Kay (Eds.), *Colour studies: A broad spectrum* (pp. 200–211). Amsterdam, The Netherlands: Benjamin.

Witzel, C., Maule, J., & Franklin, A. (in prep). Are focal colors particularly colorful?

Witzel, C., & O'Regan, J. K. (2014). Color appearance and color language depend on sensory singularities in the natural environment. *Perception, 43*(ECVP Abstract Suppl.), 67.

Wuerger, S. M., Atkinson, P., & Cropper, S. (2005). The cone inputs to the unique-hue mechanisms. *Vision Research, 45*(25–26), 3210–3223, doi:10.1016/j.visres.2005.06.016.

Wyszecki, G. (1958). Evaluation of metameric colors. *Journal of the Optical Society of America, 48*(7), 451–452, doi:10.1364/JOSA.48.000451.

Wyszecki, G., & Stiles, W. S. (1982). *Color science: Concepts and methods, quantitative data and formulae* (2nd ed.). New York, NY: Wiley.